

Geochemistry and petrology of rocks in the Decar area, central British Columbia: Petrologically constrained subdivision of the Cache Creek complex



Dejan Milidragovic^{1, a} and Ryan Grundy^{1, 2}

¹ British Columbia Geological Survey, Ministry of Energy, Mines and Petroleum Resources, Victoria, BC, V8W 9N3

² School of Earth and Ocean Sciences, University of Victoria, Victoria, BC, V8W 3P6

^a corresponding author: Dejan.Milidragovic@gov.bc.ca

Recommended citation: Milidragovic, D., and Grundy, R., 2019. Geochemistry and petrology of rocks in the Decar area, central British Columbia: Petrologically constrained subdivision of the Cache Creek complex. In: Geological Fieldwork 2018, British Columbia Ministry of Energy, Mines and Petroleum Resources, British Columbia Geological Survey Paper 2019-01, pp. 55-77.

Abstract

Upper Paleozoic to Lower Jurassic deformed rocks of the Cache Creek terrane in the Decar area, central British Columbia, include a central region of variably serpentinized or carbonate-altered ultramafic rocks (Trembleur ultramafite) that is bounded to the northeast and southwest by greenschist facies- to amphibolite facies volcano-sedimentary rocks. The predominant olivine-orthopyroxene-spinel (harzburgitic) mineralogy, and major and trace element geochemical composition of the least-altered ultramafic rocks suggest that they are remnants of a highly melt-depleted ($F \sim 0.15-0.30$) lithospheric mantle. The relatively high SiO_2 concentrations and high modal abundance of orthopyroxene in the harzburgite indicate later metasomatism, probably in a supra-subduction setting. Based on immobile and incompatible trace element abundances, we identify four geochemical suites of volcanic and shallow intrusive rocks in the Decar area. The Sowchea succession (Upper Pennsylvanian to Lower Jurassic) contains both the high-Ti alkaline and enriched to depleted tholeiitic suites, the Rubyrock igneous complex (Lower Permian to Upper Triassic) contains the HFSE-depleted suite, and local unnamed, undeformed mafic intrusions that appear to postdate assembly of the Cache Creek complex are of the calc-alkaline suite. The geochemistry of samples from the Decar area provides evidence that rocks of the Cache Creek complex consist of two fundamentally different tectono-stratigraphic assemblages. Volcanic and intrusive rocks, limestone, chert, and argillite of the Sowchea succession were likely deposited in an oceanic plateau setting. They resided on a lower plate before being juxtaposed against an upper plate consisting of the Trembleur ultramafite and overlying supracrustal rocks of the Rubyrock igneous complex.

Keywords: Cache Creek terrane, Decar, Trembleur ultramafite, Rubyrock igneous complex, Sowchea succession, Sitlika assemblage

1. Introduction

The Cache Creek terrane is a northwest-trending belt of oceanic rocks that extends for ca. 1500 km along strike in central British Columbia (Fig. 1; Monger, 1977; Nelson et al., 2013). It contains structurally imbricated and variably deformed and metamorphosed: 1) lithospheric mantle; and 2) Paleozoic to Mesozoic mafic plutonic rocks and oceanic supracrustal rocks (Monger, 1977; English and Johnston, 2005; Nelson et al., 2013; McGoldrick et al., 2017, 2018). The structural style and varied lithology of the Cache Creek terrane is widely regarded to record tectonic juxtaposition of rocks formed in disparate tectonic environments, including subduction-related fore-arc and mantle plume-related oceanic seamount and/or plateau settings (Mihalynuk et al., 1994; Struik et al., 2001; Tardy et al., 2001; Lapierre et al., 2003; English and Johnston, 2005; English et al., 2010). However, recent petrological studies in the northern part of the Cache Creek terrane offer a different perspective. McGoldrick et al. (2017) found that geochemical compositions indicate a close genetic relationship between most volcanic and intrusive rocks from northern Cache Creek terrane and adjacent ophiolite massifs, with both having evolved on the upper plate in a supra-subduction zone setting. They also found that rocks with geochemical signatures

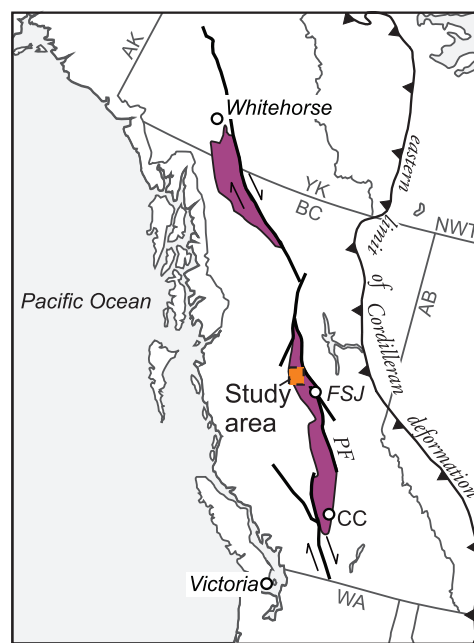


Fig. 1. Location of the study area and distribution of Cache Creek terrane (purple) in the Canadian Cordillera. Abbreviations: FSJ – town of Fort St. James; CC: village of Cache Creek; PF – Pinchi fault.

typical of intraplate oceanic basalts and related magmas (e.g., Pearce, 2008) are volumetrically minor (McGoldrick et al., 2017), casting doubt on the proposition of Tardy et al. (2001) and Lapierre et al. (2003) that Cache Creek terrane originated mainly as a fragmented oceanic plateau.

In this paper, we investigate the geochemistry of mantle, volcanic, and intrusive rocks from the southern segment of the Cache Creek terrane in the Decar area, approximately 100 km northwest of Fort St. James in central British Columbia (Fig. 1). We analyzed variably serpentinized and carbonate-altered rocks of the Trembleur ultramafite (Armstrong, 1949; Elliott, 1975; Paterson, 1977; Schiarizza and MacIntyre, 1998; MacIntyre and Schiarizza, 1999; Struik et al., 2001) and two supracrustal units: the Sowchea volcano-sedimentary succession (Upper Pennsylvanian to Lower Jurassic; Struik et al., 2001; Struik et al., 2007; previously assigned to the North Arm succession, Permo-Triassic, Schiarizza and MacIntyre, 1998; MacIntyre and Schiarizza, 1999) and the Rubyrock igneous complex (Lower Permian to Upper Triassic; MacIntyre and Schiarizza, 1999; Struik et al., 2001). Similar to data from northern Cache Creek terrane, our geochemical results highlight a supra-subduction zone component in the south. Our data also serve as a tool to assign outcrops to specific lithostratigraphic units that are difficult to distinguish in the field.

2. Geological setting

The Cache Creek terrane contains extensive sections of carbonate rocks, ribbon chert, argillite, coarse siliciclastic rocks, and mafic to intermediate volcanic and intrusive rocks (Monger, 1975; Mihalynuk et al., 1999; Struik et al., 2001; English et al., 2010). These rocks are temporally bracketed by Late Devonian-Middle Mississippian conodonts in northwestern British Columbia (Golding et al., 2016) and Early Jurassic radiolaria in southern Yukon (Cordey et al., 1991; Golding et al., 2016). The Cache Creek terrane collided with Stikinia by ca. 172 Ma, as indicated by the age of blueschist facies metamorphism of oceanic supracrustal rocks and the oldest post-kinematic plutons in northwestern British Columbia (Mihalynuk et al., 2004). Recent analysis of conodont collections demonstrates a significant time-dependant variation along the length of the terrane during the Pennsylvanian to Late Triassic (Golding, 2018). This finding suggests that different segments of the Cache Creek terrane were mobile relative to one another during much of the terrane's history and casts doubt on the widely accepted hypothesis of a far-travelled Cache Creek terrane that evolved in the Tethyan paleographic realm and crossed the Panthalassan ocean (Monger and Ross, 1971; Orchard et al., 2001; Nelson et al., 2013). A key feature of the Cache Creek terrane is the widespread occurrence of ultramafic rocks, interpreted as tectonic slivers that originally formed the lithospheric mantle beneath the Cache Creek ocean (Struik et al., 2001; Lapierre et al., 2003; English and Johnston, 2005; Canil et al., 2006; English et al., 2010; McGoldrick et al., 2017, 2018).

Currently, the tectonostratigraphic framework for the Cache

Creek terrane in central British Columbia includes three structurally disrupted components (MacIntyre and Schiarizza, 1999; Schiarizza and MacIntyre, 1999; Struik et al., 2001, 2007): 1) the Cache Creek complex, which contains ultramafic rocks considered mantle tectonites (Trembleur ultramafite), fine-grained, strongly deformed siliciclastic metasedimentary and less abundant volcanic rocks interpreted as accretionary complex deposits (Sowchea succession), and several predominantly carbonate rock units (Pope, Copley, and Kloch Lake successions; Struik et al., 2001); 2) the Sitlika assemblage, which is found structurally beneath ophiolitic rocks of the Cache Creek complex in the western part of the terrane, and comprises a Permo-Triassic predominantly volcanic unit interpreted as an intra-oceanic arc complex (Schiarizza and Massey, 2010) and an unconformably overlying Upper Triassic to Lower Jurassic siliciclastic succession; and 3) the Tezzeron succession, an Upper Triassic to Lower Jurassic siliciclastic unit along the eastern edge of the terrane, adjacent to the Quesnel terrane.

3. Geology of the Decar area

The central part of the Decar area is underlain by ultramafic and mafic rocks (Fig. 2) interpreted as relicts of a dismembered ophiolitic sequence (e.g., Boudier and Nicolas, 1985). The ophiolitic rocks include variably altered harzburgite, and lesser dunite and pyroxenite of the Trembleur ultramafite (cf., Struik et al., 2001), and greenschist- to amphibolite-facies mafic to ultramafic, altered and variably deformed intrusive and volcanic rocks of the Rubyrock igneous complex (MacIntyre and Schiarizza, 1999; Struik et al., 2001; Milidragovic et al., 2018a). The Rubyrock igneous complex is structurally interleaved with the western part of the Trembleur ultramafite and is widely regarded (Schiarizza and MacIntyre, 1999; Struik et al., 2001; Britten, 2017) as the crustal portion of the ophiolite. Locally, fine-grained dikes of saussuritized hornblende gabbro, which are geochemically correlative with the rocks of the Rubyrock igneous complex (see section 5.3.2.), cut the Trembleur ultramafite. A tonalite lens from the Rubyrock igneous complex yielded a U-Pb zircon crystallization age of 257 ± 5 Ma (Late Permian; Struik et al., 2001; Struik et al., 2007). This age is indistinguishable from a $258 \pm 10/-1$ Ma U-Pb zircon age of a rhyolite in the lower volcanic unit of the Sitlika assemblage, approximately 75 km north-northeast of the study area (Childe and Schiarizza, 1997; Schiarizza and Massey, 2010), and overlaps within error the maximum age (ca. 254-242 Ma) of Kutcho assemblage volcano-sedimentary rocks in the northern segment of the Cache Creek terrane (Childe and Thompson, 1997; Schiarizza, 2012). The Trembleur ultramafite is weakly to strongly altered to either serpentinite or listwanite ($\text{magnesite} \pm \text{serpentine} \pm \text{talc} \pm \text{quartz}$; Hansen et al., 2005). We assign the basalt-chert unit on the northeast flank of the Trembleur ultramafite to the Sowchea succession which, as defined by Struik et al. (2001; 2007), is a unit of Upper Pennsylvanian-Lower Jurassic fine-grained siliceous sedimentary rocks (cherty argillite and slate to muddy chert), with lesser limestone, greywacke, basalt,

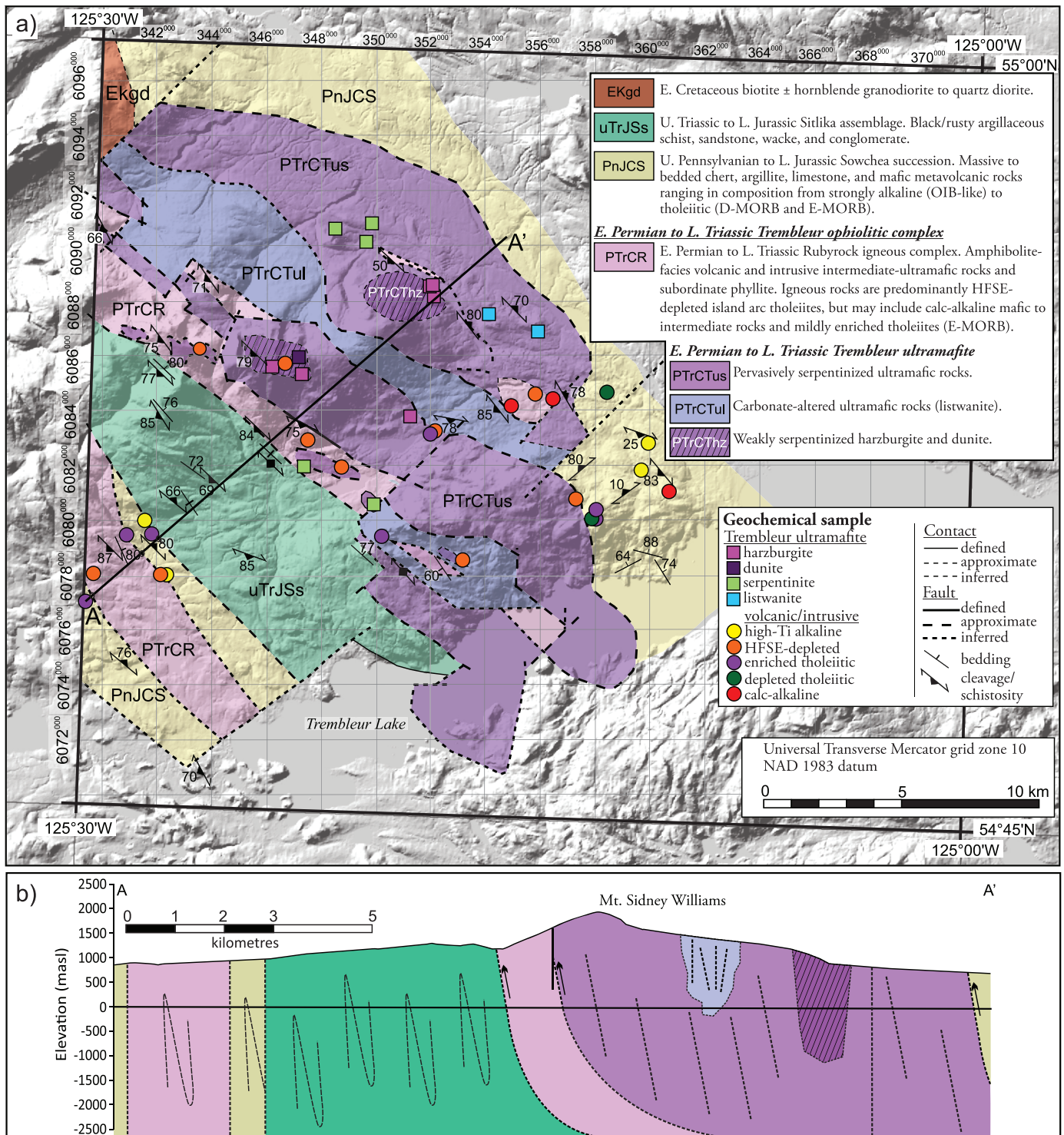


Fig. 2. a) Preliminary geology of the Decar area showing the location of samples discussed in this geochemical study. Modified from MacIntyre and Schiarizza (1999), Struik et al. (2007), and Milidragovic et al. (2018a). The hillshade terrain resource information management (TRIM) digital elevation model (DEM) base map has 25 m grid spacing. **b)** Schematic cross section (A-A') of the Decar area. Location of section is shown in Fig. 2a. Fault geometry at depth is speculative; fold pattern is ornamental.

andesite, and conglomerate containing intraformational siltstone clasts. This unit was formerly included in the North Arm succession of suspected ophiolite affinity by Schiarizza and MacIntyre (1999) and MacIntyre and Schiarizza (1999).

Immediately southwest of the ultramafic rocks are siliciclastic rocks of the upper part of Sitlika assemblage (Upper Triassic-Lower Jurassic; Schiarizza and MacIntyre, 1998; MacIntyre and Schiarizza, 1999). Farther southwest are two panels of

sedimentary and volcanic rocks that we consider part of the Sowchea succession, based on their geochemistry (see section 5.3.) and similar field appearance to rocks exposed in the northeast. Previously, these rocks, specifically a unit of mafic sills and dikes with abundant screens of basalt and chert that were interpreted as transitional between the Rubyrock complex and the North Arm succession, were included in the Rubyrock igneous complex (Schiarizza and MacIntyre, 1999; MacIntyre and Schiarizza, 1999). These Sowchea succession panels are separated by a panel of Rubyrock igneous complex rocks that we identify on the basis of geochemical data presented below (see section 5.3.2.).

The Decar area is characterized by a prominent subvertical northwest-southeast trending fabric (Fig. 2) that is consistent with northeast-southwest directed shortening (Milidragovic et al., 2018a) along northeast-dipping thrust faults (Schiarizza and MacIntyre, 1998). Shortening was also likely accompanied by significant strike-slip motion, both parallel and perpendicular to the regional fabric (Britten et al., 2017), further complicating the regional structure (Fig. 2). On the surface, observed and inferred fault contacts are subvertical and extensive drilling of the Trembleur ultramafite by FPX Nickel Corp. suggests that the ultramafic rocks extend to a minimum depth of 550 m (Voordouw and Simpson, 2018). The geometry and attitude of thrust faults at depth is unknown.

4. Analytical techniques and data quality

A total of 45 samples collected during the 2017 field season were selected for geochemical analysis at Geoscience Laboratories, Sudbury, ON. These samples span the range of rock types described by Milidragovic et al. (2018a) and include both ultramafic rocks (Table 1) and mafic- to intermediate volcanic and intrusive rocks (Table 2). The samples were prepared at the BCGS rock preparation facility before submission to Geoscience Laboratories. Before crushing in a steel jaw-crusher, obvious alteration and veins were removed from fist-sized rock samples using a diamond-studded lapidary saw. Following crushing, aliquots of each sample, weighing 30-50 g and comprising coarse (0.2-1.0 cm) rock chips and fragments, were pulverized to sub-100 μm particles using a stainless steel piston apparatus.

The samples were pulverized in an agate mill at Geoscience Laboratories. Major element oxides and selected trace element concentrations were determined using X-ray Fluorescence (XRF); trace elements were analyzed using Inductively Coupled Plasma-Mass Spectrometry (ICP-MS) following closed vessel multi-acid dissolution. Variably altered ultramafic samples were analyzed for total CO_2 and S concentrations, and a subset of serpentinite and relatively unaltered harzburgite was analyzed for platinum group element (PGE) concentrations by Ni-S fire assay.

The uncertainty in measurement, at a 95% confidence interval, is $\leq 5\%$ relative for most major element oxides whose abundance exceeds the quantification limit (defined as 3.3 times the detection limit; Fig. 3a). The relative uncertainty

in measurement of P_2O_5 ranges between 10-30% for rocks in which the absolute abundance of P_2O_5 is < 0.1 wt.%. The relative uncertainty in Co, Cu, Ni, V, and Zn as determined by XRF is typically $\leq 20\%$ at a 95% confidence interval.

Most trace element concentrations determined by ICP-MS on duplicate, in-house standard, and certified reference samples show good agreement ($\leq 15\%$ relative) with the expected values at a 95% confidence interval (Fig. 3b). However, the trace element concentrations of sample ZE15-DM-01A are up to 30% higher than those determined by high resolution-ICP-MS (HR-ICP-MS; Milidragovic et al., 2018b), suggesting that the relative uncertainty in trace element concentrations determined by ICP-MS is $\leq 30\%$. The relative uncertainty in measurement of the PGE is $< 10\%$, based on the analysis of one certified reference sample and one duplicate (Fig. 3c).

5. Petrology and geochemistry

5.1. Petrology of the Trembleur ultramafite

The least-altered rocks of the Trembleur ultramafite (LOI ≤ 10 wt.%) are spinel harzburgite with coarse or protogranular texture (Mercier and Nicholas, 1974; Harte, 1977). Partly serpentinized olivine is ≥ 3 mm across, displays kink bands and/or undulose extinction, and has curvilinear grain boundaries (Fig. 4a). Electron microprobe analysis of olivine from the Trembleur ultramafite (Grundy, 2018) demonstrated limited compositional variability (Fo=0.90-0.91; Ni=3170 \pm 780 ppm). Orthopyroxene (~ 2 -5 mm) is subhedral to anhedral and commonly contains exsolution lamellae of clinopyroxene, some of which have been deformed. Bastite alteration rims around orthopyroxene vary in thickness, but correlate broadly with the degree of serpentinization. Pervasive replacement of orthopyroxene by bastite is typically also accompanied by secondary black spinel. Rare subhedral clinopyroxene grains (< 1 mm; Fig. 4b) commonly contain cleavage-parallel exsolution of thin, closely spaced (< 10 μm) laminae of secondary spinel. Primary spinel is characteristically irregular (Fig. 4a), with a vermicular, interstitial habit and commonly displays holly-leaf texture in orthopyroxene porphyroclasts. Primary spinel is medium brown to dark red with Cr-numbers ($(\text{Cr}/(\text{Cr}+\text{Fe}^{3+}+\text{Al}))$) between 0.22 and 0.30 and Mg-numbers ($(\text{Mg}/(\text{Mg}+\text{Fe}^{2+}))$) between 0.69 and 0.73 (Grundy, 2018). Secondary black magnetite haloes around primary spinel are in all samples. Sulphide occurs in trace quantities as small (< 50 μm) subhedral crystals.

The peridotitic rocks of the Trembleur ultramafite were altered to either serpentinite or listwanite (magnesite \pm serpentine \pm talca \pm quartz; Hansen et al., 2005; Figs. 4c and d). Progressive hydration (LOI=10-14 wt.%) of harzburgite resulted in the replacement of olivine by serpentine \pm brucite \pm magnetite, and formation of microscopic awaruite (Ni_3Fe ; Britten, 2017; Milidragovic et al., 2018). Trace amounts of heazlewoodite (Ni_3S_2), pentlandite ($(\text{Fe},\text{Ni})_9\text{S}_8$), cobalt-pentlandite, millerite (NiFe), and wairauite (CoFe) occur in the serpentinites of the Decar area (Figs. 4e-f; C. Lawley, pers. comm., 2018). Ultramafic rocks in the south-central and eastern portion of the

Table 1. Major and trace element composition of the Trembleur ultramafite.

| Sample | DMI17-5-9 | DMI17-5-10 | DMI17-9-3 | DMI17-9-7A | DMI17-9-11 | DMI17-16-3C | RGR17-16-6 |
|------------------------------------|-------------|-------------|-------------|-------------|------------|-------------|-------------|
| Lithology | harzburgite | harzburgite | harzburgite | harzburgite | dunite | harzburgite | harzburgite |
| Easting | 352040 | 351934 | 347289 | 346215 | 347175 | 352085 | 351229 |
| Northing | 6088686 | 6088643 | 6085450 | 6085724 | 6086068 | 6088282 | 6083981 |
| Major elements (wt.%) | | | | | | | |
| SiO ₂ | 0.04 | 39.40 | 39.74 | 40.47 | 41.64 | 37.3 | 38.32 |
| TiO ₂ | 0.001 | 0.02 | 0.01 | 0.01 | 0.02 | 0.01 | 0.01 |
| Al ₂ O ₃ | 0.02 | 1.03 | 0.79 | 1.34 | 1.23 | 0.06 | 0.48 |
| Fe ₂ O ₃ (T) | 0.01 | 8.18 | 7.97 | 8.43 | 8.45 | 7.61 | 7.89 |
| MnO | 0.02 | 0.121 | 0.111 | 0.119 | 0.135 | 0.109 | 0.114 |
| MgO | 0.01 | 40.21 | 40.81 | 39.51 | 38.71 | 46.37 | 40.66 |
| CaO | 0.006 | 1.819 | 1.286 | 1.345 | 2.614 | 0.053 | 0.51 |
| Na ₂ O | 0.02 | <0.02 | <0.02 | <0.02 | <0.02 | <0.02 | <0.02 |
| K ₂ O | 0.01 | 0.01 | 0.01 | 0.01 | 0.01 | 0.01 | 0.01 |
| P ₂ O ₅ | 0.002 | 0.002 | <0.002 | 0.003 | 0.003 | 0.002 | 0.002 |
| Cr ₂ O ₃ | 0.002 | 0.426 | 0.367 | 0.453 | 0.381 | 0.375 | 0.366 |
| LOI | - | 8.51 | 8.93 | 7.29 | 5.41 | 7.08 | 10.28 |
| CO ₂ | 0.023 | 0.142 | 0.160 | 0.303 | 0.274 | 0.321 | 0.234 |
| S | 0.003 | 0.008 | 0.009 | 0.02 | 0.005 | 0.012 | 0.009 |
| Total | 0.01 | 99.68 | 99.98 | 99.01 | 98.55 | 98.94 | 99.82 |
| Trace elements (ppm) | | | | | | | |
| Ni ^a | 9 | 2238 | 2386 | 2315 | 2198 | 2870 | 2318 |
| V ^a | 8 | 41 | 40 | 51 | 51 | 12 | 31 |
| Co ^a | 12 | 110 | 108 | 116 | 117 | 128 | 115 |
| Cu | 1.4 | 11.3 | 15.2 | 20.1 | 18.9 | <1.4 | 3.3 |
| Zn | 1.8 | 67.7 | 63.2 | 76.1 | 70.3 | 49.2 | 47.1 |
| Cd | 0.013 | 0.022 | 0.024 | 0.027 | 0.013 | <0.013 | 0.013 |
| Sc | 1.1 | 11 | 10 | 13 | 13 | 3 | 9 |
| Ga | 0.04 | 1.01 | 0.89 | 1.36 | 1.07 | 0.21 | 0.57 |
| Li | 0.4 | 0.7 | 0.4 | 1.8 | 1.7 | 1 | 1.5 |
| Be | 0.04 | 0.08 | 0.08 | 0.07 | 0.12 | 0.07 | 0.07 |
| Mo | 0.08 | 0.13 | 0.15 | 0.16 | 0.47 | 0.18 | 0.13 |
| In | 0.0018 | 0.0076 | 0.0071 | 0.008 | 0.009 | 0.0047 | 0.0045 |
| Sn | 0.16 | <0.16 | <0.16 | <0.16 | 0.29 | <0.16 | <0.16 |
| Sb | 0.04 | <0.04 | <0.04 | 0.37 | 0.05 | 0.07 | <0.04 |
| W | 0.05 | <0.05 | <0.05 | 0.18 | 0.08 | 0.06 | <0.05 |
| Tl | 0.002 | <0.002 | 0.002 | 0.002 | 0.002 | <0.002 | 0.002 |
| Pb | 0.18 | <0.18 | <0.18 | <0.18 | 0.26 | <0.18 | <0.18 |
| Bi | 0.47 | <0.47 | <0.47 | <0.47 | <0.47 | <0.47 | <0.47 |
| Cs | 0.013 | <0.013 | <0.013 | 0.036 | <0.013 | <0.013 | <0.013 |
| Rb | 0.11 | <0.11 | 0.13 | 0.22 | 0.12 | <0.11 | 0.17 |
| Ba | 0.8 | <0.8 | <0.8 | 0.8 | 1.0 | <0.8 | <0.8 |
| Sr | 0.6 | <0.6 | 0.6 | 1.0 | <0.6 | <0.6 | <0.6 |
| Nb | 0.028 | 0.052 | 0.049 | 0.102 | 0.046 | 0.035 | 0.056 |
| Zr | 6 | <6 | 7 | <6 | <6 | <6 | <6 |
| Y | 0.05 | 0.39 | 0.24 | 0.41 | 0.58 | <0.05 | 0.08 |
| Th | 0.018 | <0.018 | <0.018 | <0.018 | <0.018 | <0.018 | <0.018 |
| U | 0.011 | <0.011 | <0.011 | <0.011 | 0.15 | <0.011 | <0.011 |
| Ta | 0.007 | 0.011 | 0.016 | 0.012 | 0.025 | 0.033 | <0.007 |
| La | 0.1 | <0.1 | <0.1 | 0.1 | 0.1 | <0.1 | <0.1 |
| Ce | 0.12 | <0.12 | <0.12 | 0.13 | <0.12 | <0.12 | <0.12 |
| Pr | 0.014 | <0.014 | <0.014 | <0.014 | 0.014 | <0.014 | <0.014 |
| Nd | 0.06 | <0.06 | 0.06 | <0.06 | <0.06 | <0.06 | <0.06 |
| Sm | 0.026 | <0.026 | <0.026 | <0.026 | <0.026 | <0.026 | <0.026 |
| Hf | 0.14 | <0.14 | 0.16 | <0.14 | <0.14 | <0.14 | <0.14 |
| Eu | 0.0031 | 0.0061 | 0.0049 | 0.0045 | 0.0062 | <0.0031 | 0.0031 |
| Gd | 0.009 | 0.028 | 0.019 | 0.020 | 0.035 | <0.009 | <0.009 |
| Tb | 0.0023 | 0.006 | 0.004 | 0.006 | 0.008 | <0.0023 | <0.0023 |
| Dy | 0.009 | 0.057 | 0.033 | 0.052 | 0.076 | <0.009 | 0.01 |
| Ho | 0.0025 | 0.015 | 0.008 | 0.015 | 0.019 | <0.0025 | 0.004 |
| Er | 0.007 | 0.050 | 0.034 | 0.053 | 0.072 | <0.007 | 0.015 |
| Tm | 0.0019 | 0.010 | 0.006 | 0.012 | 0.013 | <0.0019 | 0.003 |
| Yb | 0.009 | 0.072 | 0.049 | 0.081 | 0.095 | 0.01 | 0.024 |
| Lu | 0.002 | 0.012 | 0.009 | 0.014 | 0.016 | 0.003 | 0.004 |
| Au + PGE (ppb) | | | | | | | |
| Au ^b | 0.4 | - | 1.5 | - | 1.3 | - | 1.0 |
| Ir ^b | 0.01 | - | 3.34 | - | 3.77 | - | 3.36 |
| Pd ^b | 0.12 | - | 6.51 | - | 6.82 | - | 6.43 |
| Pt ^b | 0.17 | - | 7.10 | - | 7.48 | - | 6.40 |
| Rh ^b | 0.04 | - | 1.20 | - | 1.33 | - | 1.14 |
| Ru ^b | 0.08 | - | 6.38 | - | 7.09 | - | 6.29 |

Table 1. Continued.

| Sample | DMI17-4-5 | DMI17-10-1 | DMI17-10-2 | DMI17-10-4 | DMI17-14-1A | DMI17-5-5 | DMI17-15-6 |
|------------------------------------|--------------|--------------|--------------|--------------|--------------|------------|------------|
| Lithology | serpentinite | serpentinite | serpentinite | serpentinite | serpentinite | listwanite | listwanite |
| Easting | 349909 | 349832 | 349628 | 348503 | 347369 | 354084 | 355867 |
| Northing | 6080711 | 6090937 | 6090266 | 6090743 | 6082090 | 6087633 | 6087002 |
| Major elements (wt.%) | | | | | | | |
| SiO ₂ | 38.05 | 38.84 | 38.02 | 38.49 | 41.16 | 32.25 | 25.43 |
| TiO ₂ | 0.01 | 0.01 | 0.03 | 0.02 | 0.03 | 0.01 | 0.01 |
| Al ₂ O ₃ | 0.3 | 0.72 | 1.36 | 0.91 | 1.21 | 0.49 | 0.49 |
| Fe ₂ O ₃ (T) | 7.27 | 7.64 | 9.51 | 8.47 | 7.43 | 2.98 | 5.88 |
| MnO | 0.123 | 0.121 | 0.239 | 0.127 | 0.082 | 0.072 | 0.074 |
| MgO | 39.95 | 40.40 | 35.29 | 38.38 | 36.86 | 29.92 | 30.93 |
| CaO | 0.022 | 0.992 | 2.864 | 0.532 | 0.105 | 0.236 | 0.427 |
| Na ₂ O | <0.02 | | <0.02 | <0.02 | <0.02 | <0.02 | <0.02 |
| K ₂ O | 0.01 | 0.01 | 0.01 | 0.01 | 0.02 | 0.01 | 0.11 |
| P ₂ O ₅ | 0.007 | 0.002 | 0.002 | 0.002 | 0.007 | 0.002 | 0.002 |
| Cr ₂ O ₃ | 0.343 | 0.4 | 0.329 | 0.407 | 0.381 | 0.170 | 0.263 |
| LOI | 13.5 | 10.64 | 11.46 | 11.79 | 11.94 | 34.14 | 36.22 |
| CO ₂ | 2.609 | 1.649 | 0.818 | 0.408 | - | 34.10 | 36.19 |
| S | 0.091 | 0.009 | 0.024 | 0.009 | - | <0.003 | 0.029 |
| Total | 99.54 | 99.73 | 99.09 | 99.09 | 99.21 | 100.23 | 99.80 |
| Trace elements (ppm) | | | | | | | |
| Ni ^a | 2341 | 2464 | 1988 | 2346 | 2266 | 1140 | 1683 |
| V ^a | 19 | 37 | 56 | 36 | 45 | 16 | 24 |
| Co ^a | 109 | 114 | 122 | 111 | 104 | 49 | 84 |
| Cu | 7.5 | 16.7 | 22.1 | 14.6 | 17.3 | 3.2 | 26.2 |
| Zn | 48.9 | 56.1 | 75.8 | 60.6 | 41.4 | 36 | 47.1 |
| Cd | <0.013 | <0.013 | 0.021 | 0.015 | 0.014 | 0.014 | 0.018 |
| Sc | 8 | 9 | 15 | 10 | 13 | 5 | 7 |
| Ga | 0.88 | 0.61 | 1.00 | 0.99 | 1.12 | 0.63 | 0.67 |
| Li | 0.4 | 0.9 | 0.5 | 0.8 | 0.6 | 3.9 | 1.9 |
| Be | 0.1 | 0.07 | 0.10 | 0.09 | 0.11 | 0.13 | 0.12 |
| Mo | 0.28 | 0.13 | 0.13 | 0.21 | 0.09 | 0.15 | 0.26 |
| In | 0.0064 | 0.0067 | 0.0114 | 0.0076 | 0.008 | 0.0036 | 0.0042 |
| Sn | <0.16 | <0.16 | <0.16 | <0.16 | <0.16 | <0.16 | <0.16 |
| Sb | >28 | <0.04 | 0.11 | <0.04 | 1.34 | 1.46 | 1.21 |
| W | 9.72 | <0.05 | 0.08 | <0.05 | 0.23 | 0.93 | 0.59 |
| Tl | <0.002 | <0.002 | <0.002 | <0.002 | 0.004 | 0.004 | 0.022 |
| Pb | 0.32 | <0.18 | 0.34 | <0.18 | 0.54 | <0.18 | 0.38 |
| Bi | <0.47 | <0.47 | <0.47 | <0.47 | <0.47 | <0.47 | <0.47 |
| Cs | 0.137 | 0.015 | <0.013 | <0.013 | 0.022 | 0.131 | 0.552 |
| Rb | 0.18 | <0.11 | 0.11 | <0.11 | 0.32 | 0.29 | 2.75 |
| Ba | <0.8 | <0.8 | <0.8 | 1.7 | 7.4 | 1.2 | 3.6 |
| Sr | 1.1 | <0.6 | <0.6 | 1.8 | 5.6 | 2.1 | 2.3 |
| Nb | 0.045 | <0.028 | <0.028 | <0.028 | 0.213 | 0.117 | 0.051 |
| Zr | <6 | <6 | <6 | <6 | <6 | <6 | <6 |
| Y | 0.09 | 0.3 | 1.06 | 0.3 | 0.76 | 0.12 | 0.11 |
| Th | <0.018 | <0.018 | <0.018 | <0.018 | <0.018 | 0.027 | <0.018 |
| U | 0.02 | <0.011 | <0.011 | <0.011 | 0.02 | <0.011 | <0.011 |
| Ta | <0.007 | <0.007 | <0.007 | <0.007 | <0.007 | <0.007 | <0.007 |
| La | <0.1 | <0.1 | <0.1 | <0.1 | 0.30 | 0.1 | <0.1 |
| Ce | <0.12 | <0.12 | <0.12 | <0.12 | 0.61 | 0.20 | <0.12 |
| Pr | <0.014 | <0.014 | <0.014 | <0.014 | 0.071 | 0.019 | <0.014 |
| Nd | <0.06 | <0.06 | <0.06 | <0.06 | 0.31 | 0.06 | <0.06 |
| Sm | <0.026 | <0.026 | 0.03 | <0.026 | 0.073 | <0.026 | <0.026 |
| Hf | <0.14 | <0.14 | <0.14 | <0.14 | <0.14 | <0.14 | <0.14 |
| Eu | 0.005 | 0.005 | 0.015 | 0.004 | 0.036 | 0.004 | 0.004 |
| Gd | <0.009 | 0.015 | 0.080 | 0.015 | 0.085 | 0.013 | 0.012 |
| Tb | <0.0023 | 0.005 | 0.018 | 0.004 | 0.016 | <0.0023 | <0.0023 |
| Dy | 0.015 | 0.036 | 0.16 | 0.038 | 0.126 | 0.021 | 0.018 |
| Ho | 0.003 | 0.011 | 0.040 | 0.011 | 0.030 | 0.004 | 0.005 |
| Er | 0.012 | 0.044 | 0.135 | 0.045 | 0.095 | 0.017 | 0.019 |
| Tm | 0.003 | 0.008 | 0.024 | 0.008 | 0.016 | 0.004 | 0.004 |
| Yb | 0.023 | 0.061 | 0.177 | 0.054 | 0.106 | 0.024 | 0.026 |
| Lu | 0.004 | 0.012 | 0.029 | 0.010 | 0.017 | 0.005 | 0.006 |
| Au + PGE (ppb) | | | | | | | |
| Au ^b | 2.7 | 1.0 | 2.1 | 1.2 | - | - | - |
| Ir ^b | 3.95 | 3.38 | 2.76 | 4.17 | - | - | - |
| Pd ^b | 3.68 | 10.27 | 5.51 | 5.16 | - | - | - |
| Pt ^b | 6.43 | 7.8 | 5.89 | 7.01 | - | - | - |
| Rh ^b | 1.21 | 1.29 | 0.96 | 1.26 | - | - | - |
| Ru ^b | 6.49 | 6.47 | 5.23 | 7.31 | - | - | - |

Trace elements were analyzed by ICP-MS unless reported otherwise. ^a analyzed by XRF; ^b analyzed by Ni-S fire assay. Numbers in the first column (italics) are detection limits for individual elements. UTM coordinates for sample locations are based on Zone 10 North American datum 1983 (NAD83).

Table 2. Major and trace element composition of volcanic and shallow intrusive rocks.

| <i>Suite</i> | <i>HFSE-depleted tholeiitic</i> | | | | | | | |
|------------------------------------|---------------------------------|-----------|-----------|------------|------------|------------|-----------|-------|
| Sample | 98PSC-33-9-1 | DMI17-3-8 | DMI17-9-8 | DMI17-7-8 | DMI17-7-11 | DMI17-3-3 | DMI17-3-5 | |
| Lithology | gabbro | gabbro | gabbro | fragmental | fragmental | fragmental | basalt | |
| Easting | 343618 | 348735 | 346730 | 355776 | 357261 | 342151 | 339701 | |
| Northing | 6086409 | 6082069 | 6085645 | 6084729 | 6080910 | 6078164 | 6078209 | |
| Unit | Rubyrock | Rubyrock | Rubyrock | Rubyrock | Rubyrock | Rubyrock | Rubyrock | |
| *Former unit | - | - | - | - | - | Sowchea | - | |
| Major elements (wt.%) | | | | | | | | |
| SiO ₂ | 0.04 | 43.26 | 42.66 | 48.48 | 51.14 | 47.63 | 49.10 | 49.41 |
| TiO ₂ | 0.001 | 1.28 | 1.78 | 1.82 | 1.01 | 1.07 | 1.41 | 1.00 |
| Al ₂ O ₃ | 0.02 | 13.70 | 17.58 | 13.94 | 14.44 | 15.49 | 14.94 | 13.96 |
| Fe ₂ O ₃ (T) | 0.01 | 13.46 | 11.30 | 13.38 | 9.61 | 10.28 | 11.16 | 11.12 |
| MnO | 0.02 | 0.21 | 0.15 | 0.21 | 0.18 | 0.19 | 0.18 | 0.19 |
| MgO | 0.01 | 10.92 | 5.02 | 6.34 | 5.99 | 7.04 | 5.78 | 6.00 |
| CaO | 0.006 | 12.58 | 19.35 | 9.31 | 10.58 | 7.89 | 9.82 | 10.95 |
| Na ₂ O | 0.02 | 1.61 | 0.28 | 3.78 | 2.54 | 3.79 | 3.86 | 2.94 |
| K ₂ O | 0.01 | 0.30 | 0.06 | 0.26 | 0.34 | 0.65 | 0.08 | 1.09 |
| P ₂ O ₅ | 0.002 | 0.13 | 0.14 | 0.15 | 0.09 | 0.09 | 0.13 | 0.14 |
| Cr ₂ O ₃ | 0.002 | 0.06 | 0.01 | 0.01 | 0.03 | 0.04 | 0.02 | 0.02 |
| LOI | - | 2.13 | 1.88 | 2.03 | 3.17 | 5.18 | 2.63 | 2.55 |
| Total | 0.01 | 99.66 | 100.21 | 99.71 | 99.12 | 99.36 | 99.12 | 99.38 |
| Trace elements (ppm) | | | | | | | | |
| Ni ^a | 9 | 161 | 37 | 32 | 73 | 85 | 75 | 41 |
| V ^a | 8 | 362 | 350 | 379 | 255 | 291 | 310 | 265 |
| Co ^a | 12 | 48 | 35 | 47 | 37 | 34 | 36 | 50 |
| Cu | 1.4 | 27 | 62 | 53 | 36 | 35 | 21 | 40 |
| Zn | 1.8 | 109 | 96 | 106 | 97 | 91 | 86 | 89 |
| Cd | 0.013 | 0.14 | 0.28 | 0.16 | 0.18 | 0.094 | 0.12 | 0.21 |
| Sc | 1.1 | 54 | 40 | 41 | 35 | 40 | 39 | 52 |
| Ga | 0.04 | 17 | 21 | 19 | 18 | 20 | 19 | 15 |
| Li | 0.4 | 8 | 1 | 9 | 8 | 13 | 9 | 14 |
| Be | 0.04 | 0.38 | 0.41 | 0.56 | 0.44 | 0.38 | 0.55 | 0.46 |
| Mo | 0.08 | 0.31 | 0.53 | 0.36 | 0.33 | 1.09 | 0.35 | 0.17 |
| In | 0.0018 | 0.083 | 0.084 | 0.092 | 0.056 | 0.066 | 0.078 | 0.064 |
| Sn | 0.16 | 0.67 | 0.69 | 1.03 | 0.81 | 0.87 | 0.89 | 0.48 |
| Sb | 0.04 | <0.04 | 0.5 | 0.05 | 0.75 | 0.46 | 0.16 | 0.17 |
| W | 0.05 | 0.07 | 0.34 | 0.08 | 0.21 | 0.29 | 0.16 | 0.1 |
| Tl | 0.002 | 0.028 | 0.008 | 0.052 | 0.071 | 0.106 | 0.003 | 0.052 |
| Pb | 0.18 | 0.3 | 1.02 | 0.53 | 0.92 | 1.91 | 0.5 | 0.31 |
| Bi | 0.47 | <0.47 | <0.47 | <0.47 | <0.47 | <0.47 | <0.47 | <0.47 |
| Cs | 0.013 | 0.11 | 0.06 | 1.29 | 0.13 | 0.19 | 0.04 | 0.64 |
| Rb | 0.11 | 2.8 | 0.6 | 6.1 | 7.1 | 12.3 | 0.5 | 24.2 |
| Ba | 0.8 | 16 | 22 | 28 | 52 | 198 | 23 | 36 |
| Sr | 0.6 | 66 | 54 | 143 | 72 | 122 | 269 | 112 |
| Nb | 0.028 | 1.0 | 1.9 | 1.6 | 0.9 | 1.3 | 2.0 | 2.2 |
| Zr | 6 | 53 | 106 | 109 | 66 | 70 | 95 | 59 |
| Y | 0.05 | 30.6 | 38.5 | 40.8 | 23.7 | 29.0 | 32.9 | 31.6 |
| Th | 0.018 | 0.17 | 0.16 | 0.16 | 0.10 | 0.14 | 0.23 | 0.16 |
| U | 0.011 | 0.17 | 0.08 | 0.07 | 0.08 | 0.13 | 0.10 | 0.26 |
| Ta | 0.007 | 0.07 | 0.13 | 0.11 | 0.06 | 0.09 | 0.13 | 0.14 |
| La | 0.1 | 3.10 | 4.10 | 3.80 | 2.00 | 2.40 | 3.90 | 3.30 |
| Ce | 0.12 | 9.41 | 12.43 | 12.37 | 6.58 | 7.41 | 11.38 | 7.61 |
| Pr | 0.014 | 1.71 | 2.26 | 2.19 | 1.21 | 1.34 | 1.99 | 1.47 |
| Nd | 0.06 | 9.26 | 12.23 | 12.01 | 6.84 | 7.69 | 10.28 | 7.80 |
| Sm | 0.026 | 3.27 | 4.22 | 4.34 | 2.46 | 2.77 | 3.48 | 2.81 |
| Hf | 0.14 | 1.75 | 2.98 | 3.15 | 1.87 | 1.92 | 2.55 | 1.61 |
| Eu | 0.0031 | 1.18 | 1.71 | 1.52 | 0.960 | 1.07 | 1.37 | 1.02 |
| Gd | 0.009 | 4.40 | 5.65 | 5.88 | 3.49 | 3.95 | 4.83 | 4.06 |
| Tb | 0.0023 | 0.783 | 0.992 | 1.030 | 0.610 | 0.677 | 0.835 | 0.740 |
| Dy | 0.009 | 5.38 | 6.76 | 7.17 | 4.18 | 4.79 | 5.65 | 5.13 |
| Ho | 0.0025 | 1.14 | 1.46 | 1.53 | 0.87 | 1.02 | 1.20 | 1.12 |
| Er | 0.007 | 3.36 | 4.37 | 4.58 | 2.65 | 3.09 | 3.57 | 3.31 |
| Tm | 0.0019 | 0.493 | 0.630 | 0.661 | 0.382 | 0.452 | 0.512 | 0.476 |
| Yb | 0.009 | 3.27 | 4.09 | 4.34 | 2.51 | 2.92 | 3.39 | 3.11 |
| Lu | 0.002 | 0.493 | 0.619 | 0.655 | 0.381 | 0.449 | 0.496 | 0.464 |

Table 2. Continued.

| Suite | <i>HFSE-depleted tholeiitic</i> | | | <i>High-Ti alkaline</i> | | | |
|------------------------------------|---------------------------------|------------|------------|-------------------------|------------|-----------|-----------|
| Sample | DMI17-4-16 | DMI17-14-9 | DMI17-5-2 | DMI17-3-4 | DMI17-2-12 | DMI17-8-4 | DMI17-8-5 |
| Lithology | gabbro | basalt | fragmental | basalt | basalt | basalt | basalt |
| Easting | 353146 | 347506 | 352136 | 342367 | 341575 | 359890 | 359636 |
| Northing | 6078686 | 6083053 | 6083383 | 6078155 | 6080135 | 6082947 | 6081964 |
| Unit | Rubyrock | Rubyrock | Rubyrock | Sowchea | Sowchea | Sowchea | Sowchea |
| *Former unit | Sowchea | - | - | - | - | - | - |
| Major elements (wt.%) | | | | | | | |
| SiO ₂ | 42.12 | 45.30 | 49.11 | 45.88 | 32.85 | 38.04 | 55.59 |
| TiO ₂ | 0.29 | 1.32 | 1.27 | 2.83 | 3.68 | 2.09 | 1.41 |
| Al ₂ O ₃ | 18.45 | 15.42 | 13.36 | 14.49 | 17.23 | 14.3 | 18.07 |
| Fe ₂ O ₃ (T) | 6.59 | 12.66 | 15.29 | 12.4 | 13.49 | 13.45 | 6.55 |
| MnO | 0.14 | 0.21 | 0.27 | 0.16 | 0.18 | 0.11 | 0.14 |
| MgO | 9.38 | 7.76 | 5.77 | 6.14 | 5.38 | 5.67 | 3.17 |
| CaO | 17.90 | 12.16 | 7.82 | 9.36 | 14.62 | 4.56 | 1.99 |
| Na ₂ O | 0.26 | 1.61 | 3.36 | 2.95 | 1.32 | 2.47 | 5.67 |
| K ₂ O | 0.28 | 0.75 | 0.41 | 0.6 | 0.62 | 1.62 | 1.89 |
| P ₂ O ₅ | 0.02 | 0.09 | 0.11 | 0.59 | 0.96 | 0.37 | 0.75 |
| Cr ₂ O ₃ | 0.13 | 0.02 | 0.00 | 0.02 | 0.01 | 0.03 | 0.09 |
| LOI | 3.95 | 2.52 | 2.69 | 3.3 | 9.24 | 16.76 | 3.93 |
| Total | 99.51 | 99.87 | 99.48 | 98.74 | 99.62 | 99.56 | 99.36 |
| Trace elements (ppm) | | | | | | | |
| Ni ^a | 149 | 54 | 35 | 79 | 99 | 90 | 19 |
| V ^a | 161 | 392 | 474 | 196 | 232 | 141 | 131 |
| Co ^a | 41 | 51 | 52 | 37 | 42 | 42 | 13 |
| Cu | 128 | 276 | 237 | 53 | 7 | 56 | 53 |
| Zn | 38 | 110 | 121 | 115 | 163 | 219 | 89 |
| Cd | 0.16 | 0.47 | 0.07 | 0.17 | 0.30 | 0.08 | 0.03 |
| Sc | 40 | 47 | 56 | 21 | 23 | 22 | 43 |
| Ga | 15 | 20 | 18 | 24 | 31 | 16 | 16 |
| Li | 16 | 12 | 9 | 21 | 48 | 34 | 20 |
| Be | 0.22 | 0.50 | 0.33 | 1.06 | 0.89 | 0.82 | 1.12 |
| Mo | 0.27 | 0.2 | 0.17 | 2.08 | 0.94 | 0.13 | 1.01 |
| In | 0.028 | 0.109 | 0.096 | 0.088 | 0.109 | 0.044 | 0.059 |
| Sn | <0.16 | 1.06 | 0.70 | 2.28 | 2.43 | 0.84 | 1.14 |
| Sb | 1.29 | 0.87 | 0.16 | 0.41 | 0.72 | 0.84 | 0.39 |
| W | 0.16 | 0.24 | 0.10 | 0.4 | 0.81 | 5.95 | 0.87 |
| Tl | 0.026 | 0.107 | 0.063 | 0.121 | 0.067 | 0.349 | 0.35 |
| Pb | 1.33 | 1.83 | 0.58 | 2.06 | 6.02 | 1.74 | 1.34 |
| Bi | <0.47 | <0.47 | <0.47 | <0.47 | <0.47 | <0.47 | <0.47 |
| Cs | 0.04 | 0.18 | 0.96 | 0.56 | 0.30 | 1.62 | 1.13 |
| Rb | 4.3 | 12.3 | 8.7 | 15.3 | 12.5 | 41.4 | 38.2 |
| Ba | 56 | 351 | 66 | 79 | 461 | 881 | 906 |
| Sr | 206 | 405 | 219 | 240 | 409 | 193 | 66 |
| Nb | 0.4 | 1.1 | 1.0 | 49.9 | 41.6 | 29.5 | 29.7 |
| Zr | 10 | 47 | 71 | 292 | 314 | 169 | 118 |
| Y | 7.56 | 32.72 | 42.2 | 33.58 | 35.77 | 20.97 | 33.37 |
| Th | 0.04 | 0.02 | 0.111 | 4.526 | 2.175 | 2.03 | 2.575 |
| U | 0.01 | 0.02 | 0.03 | 1.45 | 0.54 | 0.47 | 0.59 |
| Ta | 0.02 | 0.07 | 0.06 | 3.14 | 2.67 | 1.54 | 1.85 |
| La | 0.80 | 1.50 | 1.50 | 37.60 | 33.70 | 11.90 | 17.30 |
| Ce | 1.74 | 6.11 | 4.83 | 82.3 | 75.84 | 24.33 | 27.22 |
| Pr | 0.34 | 1.28 | 0.98 | 10.32 | 10.38 | 3.46 | 4.23 |
| Nd | 1.74 | 7.62 | 6.02 | 42.49 | 45.52 | 15.83 | 17.53 |
| Sm | 0.75 | 3.03 | 2.83 | 9.07 | 10.30 | 3.80 | 3.99 |
| Hf | 0.33 | 1.52 | 2.11 | 6.68 | 7.52 | 3.98 | 2.72 |
| Eu | 0.417 | 1.213 | 1.115 | 2.78 | 3.53 | 1.19 | 1.29 |
| Gd | 1.11 | 4.44 | 4.85 | 8.27 | 9.49 | 3.97 | 4.36 |
| Tb | 0.200 | 0.799 | 0.938 | 1.19 | 1.34 | 0.584 | 0.713 |
| Dy | 1.33 | 5.53 | 6.89 | 6.87 | 7.62 | 3.59 | 4.71 |
| Ho | 0.29 | 1.18 | 1.56 | 1.24 | 1.33 | 0.74 | 0.99 |
| Er | 0.83 | 3.595 | 4.90 | 3.27 | 3.39 | 2.29 | 2.97 |
| Tm | 0.117 | 0.524 | 0.728 | 0.428 | 0.429 | 0.323 | 0.425 |
| Yb | 0.75 | 3.45 | 4.89 | 2.63 | 2.58 | 2.13 | 2.74 |
| Lu | 0.110 | 0.524 | 0.742 | 0.368 | 0.345 | 0.328 | 0.419 |

Table 2. Continued.

| Suite | <i>Enriched tholeiitic</i> | | | | | | |
|------------------------------------|----------------------------|------------|------------|------------|------------|-----------|-----------|
| Sample | DMI17-2-9 | DMI17-2-15 | DMI17-4-10 | DMI17-18-5 | DMI17-5-1A | DMI17-1-2 | DMI17-1-7 |
| Lithology | basalt | basalt | fragmental | basalt | fragmental | basalt | basalt |
| Easting | 341827 | 339417 | 350198 | 340913 | 351965 | 358000 | 357993 |
| Northing | 6079643 | 6077194 | 6079547 | 6079612 | 6083272 | 6080523 | 6080182 |
| Unit | Sowchea | Sowchea | Rubyrock? | Sowchea | Rubyrock? | Sowchea | Sowchea |
| *Former unit | - | Rubyrock | Trembleur | - | Rubyrock | - | - |
| Major elements (wt.%) | | | | | | | |
| SiO ₂ | 49.89 | 49.28 | 45.7 | 54.33 | 49.59 | 50.98 | 57.12 |
| TiO ₂ | 1.12 | 1.37 | 1.90 | 0.64 | 0.56 | 0.52 | 0.40 |
| Al ₂ O ₃ | 13.35 | 13.9 | 14.35 | 11.49 | 18.55 | 14.59 | 12.43 |
| Fe ₂ O ₃ (T) | 12.49 | 12.16 | 12.55 | 9.13 | 9.39 | 8.49 | 5.74 |
| MnO | 0.19 | 0.21 | 0.22 | 0.16 | 0.17 | 0.16 | 0.10 |
| MgO | 6.51 | 6.58 | 6.03 | 8.43 | 5.19 | 8.40 | 6.97 |
| CaO | 9.72 | 9.11 | 10.53 | 8.90 | 7.95 | 6.20 | 9.81 |
| Na ₂ O | 3.27 | 3.38 | 3.14 | 3.33 | 4.47 | 2.09 | 3.96 |
| K ₂ O | 0.25 | 0.16 | 0.07 | 0.54 | 0.41 | 3.39 | 0.08 |
| P ₂ O ₅ | 0.11 | 0.12 | 0.22 | 0.05 | 0.13 | 0.08 | 0.04 |
| Cr ₂ O ₃ | 0.02 | 0.01 | 0.01 | 0.13 | 0.01 | 0.03 | 0.01 |
| LOI | 2.03 | 3.02 | 5.36 | 1.85 | 3.12 | 4.33 | 2.38 |
| Total | 98.96 | 99.28 | 100.07 | 99.01 | 99.56 | 99.41 | 99.04 |
| Trace elements (ppm) | | | | | | | |
| Ni ^a | 60 | 36 | 32 | 244 | 53 | 72 | 115 |
| V ^a | 331 | 317 | 318 | 225 | 125 | 206 | 98 |
| Co ^a | 46 | 55 | 44 | 44 | 33 | 39 | 30 |
| Cu | 90 | 102 | 16 | 217 | 79 | 139 | 58 |
| Zn | 99 | 96 | 92 | 65 | 74 | 66 | 50 |
| Cd | 0.11 | 0.09 | 0.16 | 0.11 | 0.07 | 0.15 | 0.18 |
| Sc | 48 | 57 | 45 | 39 | 28 | 36 | 21 |
| Ga | 15 | 15 | 20 | 11 | 15 | 14 | 11 |
| Li | 11 | 10 | 15 | 7 | 13 | 16 | 3 |
| Be | 0.4 | 0.58 | 1.05 | 0.66 | 0.32 | 0.44 | 0.16 |
| Mo | 0.09 | 0.2 | 0.44 | 0.36 | 0.18 | <0.08 | 0.09 |
| In | 0.075 | 0.081 | 0.077 | 0.054 | 0.049 | 0.055 | 0.025 |
| Sn | 0.74 | 0.74 | 1.29 | 0.60 | 0.36 | 0.31 | 0.33 |
| Sb | 0.64 | 0.22 | 0.3 | 1.11 | 0.22 | 0.34 | 0.18 |
| W | 0.31 | 0.19 | 0.17 | 0.25 | 0.14 | 0.30 | 0.10 |
| Tl | 0.016 | 0.015 | 0.009 | 0.055 | 0.058 | 0.686 | 0.007 |
| Pb | 0.79 | 0.52 | 0.76 | 1.99 | 0.45 | 0.18 | 0.58 |
| Bi | <0.47 | <0.47 | <0.47 | <0.47 | <0.47 | <0.47 | <0.47 |
| Cs | 0.05 | 0.06 | 0.04 | 0.22 | 0.12 | 1.50 | 0.02 |
| Rb | 3.2 | 2.2 | 1.0 | 9.6 | 7.4 | 66.0 | 0.8 |
| Ba | 45 | 45 | 12 | 214 | 176 | 1302 | 32 |
| Sr | 188 | 61 | 114 | 88 | 90 | 32 | 101 |
| Nb | 4.0 | 3.9 | 10.8 | 2.5 | 4.2 | 2.4 | 3.0 |
| Zr | 75 | 85 | 163 | 38 | 47 | 32 | 48 |
| Y | 30.24 | 33.64 | 33.23 | 16.54 | 15.91 | 15.24 | 11.14 |
| Th | 0.288 | 0.29 | 0.861 | 0.187 | 0.218 | 0.147 | 0.617 |
| U | 0.34 | 0.10 | 0.48 | 0.04 | 0.08 | 0.05 | 0.82 |
| Ta | 0.26 | 0.25 | 0.70 | 0.16 | 0.23 | 0.14 | 0.21 |
| La | 4.20 | 3.90 | 11.30 | 2.00 | 3.40 | 1.60 | 4.60 |
| Ce | 10.59 | 10.82 | 27.31 | 4.77 | 7.84 | 3.94 | 7.79 |
| Pr | 1.68 | 1.76 | 3.95 | 0.78 | 1.13 | 0.70 | 1.29 |
| Nd | 8.44 | 9.13 | 18.02 | 3.91 | 4.99 | 3.55 | 5.31 |
| Sm | 2.85 | 3.24 | 4.92 | 1.39 | 1.41 | 1.23 | 1.44 |
| Hf | 2.00 | 2.25 | 3.85 | 1.06 | 1.20 | 0.87 | 1.29 |
| Eu | 1.12 | 1.21 | 1.61 | 0.530 | 0.578 | 0.467 | 0.503 |
| Gd | 3.92 | 4.57 | 5.64 | 2.04 | 1.85 | 1.85 | 1.71 |
| Tb | 0.724 | 0.823 | 0.930 | 0.376 | 0.339 | 0.347 | 0.306 |
| Dy | 5.09 | 5.77 | 6.05 | 2.64 | 2.48 | 2.55 | 2.14 |
| Ho | 1.12 | 1.24 | 1.23 | 0.58 | 0.56 | 0.58 | 0.45 |
| Er | 3.43 | 3.72 | 3.63 | 1.82 | 1.78 | 1.80 | 1.35 |
| Tm | 0.503 | 0.545 | 0.515 | 0.278 | 0.278 | 0.277 | 0.199 |
| Yb | 3.32 | 3.56 | 3.39 | 1.90 | 1.92 | 1.87 | 1.30 |
| Lu | 0.503 | 0.538 | 0.503 | 0.292 | 0.311 | 0.293 | 0.202 |

Table 2. Continued.

| Suite | <i>Depleted tholeiitic</i> | | <i>Calc-alkaline</i> | | |
|------------------------------------|----------------------------|-------------|----------------------|-----------------|-----------------|
| Sample | DMI17-15-7 | DMI17-1-5 | DMI17-8-11 | DMI17-15-3 | DMI17-7-6 |
| Lithology | gabbro | ol. cpxite. | gabbro | qz. diorite | hornblendite |
| Easting | 358303 | 357841 | 360652 | 356417 | 354903 |
| Northing | 6084840 | 6080196 | 6081188 | 6084553 | 6084296 |
| Unit | Sowchea | Sowchea | Late intrusion | Late intrusion | Late intrusion |
| *Former unit | - | - | Sowchea (S'01) | Rubyrock (S'01) | Rubyrock (S'01) |
| Major elements (wt.%) | | | | | |
| SiO ₂ | 49.32 | 42.70 | 46.55 | 62.55 | 43.51 |
| TiO ₂ | 0.58 | 0.44 | 0.78 | 0.34 | 0.70 |
| Al ₂ O ₃ | 15.75 | 8.80 | 12.55 | 15.40 | 11.62 |
| Fe ₂ O ₃ (T) | 9.41 | 11.46 | 7.52 | 2.93 | 9.57 |
| MnO | 0.16 | 0.21 | 0.14 | 0.07 | 0.17 |
| MgO | 7.16 | 19.50 | 10.47 | 1.01 | 17.76 |
| CaO | 10.38 | 8.55 | 10.36 | 3.54 | 8.93 |
| Na ₂ O | 3.28 | 0.09 | 3.10 | 8.74 | 1.20 |
| K ₂ O | 0.05 | 0.26 | 0.85 | 0.29 | 0.51 |
| P ₂ O ₅ | 0.05 | 0.04 | 0.15 | 0.16 | 0.15 |
| Cr ₂ O ₃ | 0.04 | 0.37 | 0.09 | <0.002 | 0.15 |
| LOI | 3.07 | 6.25 | 6.63 | 3.41 | 4.69 |
| Total | 99.25 | 98.66 | 99.21 | 98.45 | 99.00 |
| Trace elements (ppm) | | | | | |
| Ni ^a | 62 | 921 | 223 | <9 | 575 |
| V ^a | 240 | 192 | 200 | 44 | 170 |
| Co ^a | 37 | 104 | 40 | <12 | 66 |
| Cu | 29 | 86 | 9 | 16 | 15 |
| Zn | 67 | 105 | 55 | 26 | 80 |
| Cd | 0.08 | 0.24 | 0.05 | 0.30 | 0.08 |
| Sc | 50 | 39 | 38 | 7 | 25 |
| Ga | 14 | 9 | 13 | 15 | 12 |
| Li | 8 | 57 | 41 | 1 | 24 |
| Be | 0.19 | 0.28 | 1.59 | 1.17 | 0.90 |
| Mo | 0.12 | 0.1 | 0.1 | <0.08 | 0.45 |
| In | 0.052 | 0.043 | 0.042 | 0.013 | 0.043 |
| Sn | 0.34 | <0.16 | 0.55 | 0.64 | 0.29 |
| Sb | 0.46 | 1.99 | 0.61 | 0.33 | 0.29 |
| W | 0.21 | 0.05 | 0.36 | 6.87 | 0.23 |
| Tl | 0.003 | 0.029 | 0.169 | 0.020 | 0.043 |
| Pb | 0.40 | 0.18 | 1.29 | 5.79 | 0.45 |
| Bi | <0.47 | <0.47 | <0.47 | 0.61 | <0.47 |
| Cs | 0.02 | 0.18 | 1.08 | 0.05 | 0.35 |
| Rb | 0.5 | 4.1 | 21.8 | 3.0 | 7.8 |
| Ba | 21 | 91 | 217 | 203 | 320 |
| Sr | 47 | 7 | 482 | 480 | 104 |
| Nb | 1.1 | 1.0 | 7.0 | 2.0 | 4.9 |
| Zr | 32 | 21 | 63 | 89 | 63 |
| Y | 20.31 | 13.7 | 16.74 | 11.11 | 14.07 |
| Th | 0.094 | 0.075 | 1.268 | 0.955 | 0.5 |
| U | 0.03 | 0.11 | 0.58 | 0.59 | 0.22 |
| Ta | 0.06 | 0.06 | 0.32 | 0.11 | 0.28 |
| La | 1.20 | 1.10 | 29.60 | 7.00 | 7.60 |
| Ce | 3.06 | 2.52 | 75.81 | 16.78 | 18.22 |
| Pr | 0.57 | 0.45 | 10.47 | 2.31 | 2.57 |
| Nd | 3.16 | 2.35 | 39.50 | 9.97 | 11.28 |
| Sm | 1.40 | 0.97 | 5.44 | 2.12 | 2.56 |
| Hf | 0.94 | 0.63 | 1.74 | 2.57 | 1.59 |
| Eu | 0.565 | 0.342 | 1.332 | 0.661 | 0.827 |
| Gd | 2.28 | 1.57 | 3.76 | 1.88 | 2.61 |
| Tb | 0.455 | 0.309 | 0.541 | 0.290 | 0.407 |
| Dy | 3.31 | 2.32 | 3.24 | 1.85 | 2.69 |
| Ho | 0.76 | 0.53 | 0.64 | 0.38 | 0.53 |
| Er | 2.357 | 1.655 | 1.78 | 1.15 | 1.54 |
| Tm | 0.351 | 0.251 | 0.250 | 0.170 | 0.216 |
| Yb | 2.37 | 1.76 | 1.65 | 1.18 | 1.39 |
| Lu | 0.363 | 0.274 | 0.243 | 0.182 | 0.211 |

Trace elements were analyzed by ICP-MS unless reported otherwise. ^a analyzed by XRF. Numbers in first column (italics) are detection limits for individual elements. UTM coordinates for sample locations are based on Zone 10 North American datum 1983 (NAD83).

*Former stratigraphic rock unit assignment as used by Struik et al. (2007) is given for rock samples that were reassigned to different units based on their geochemistry.

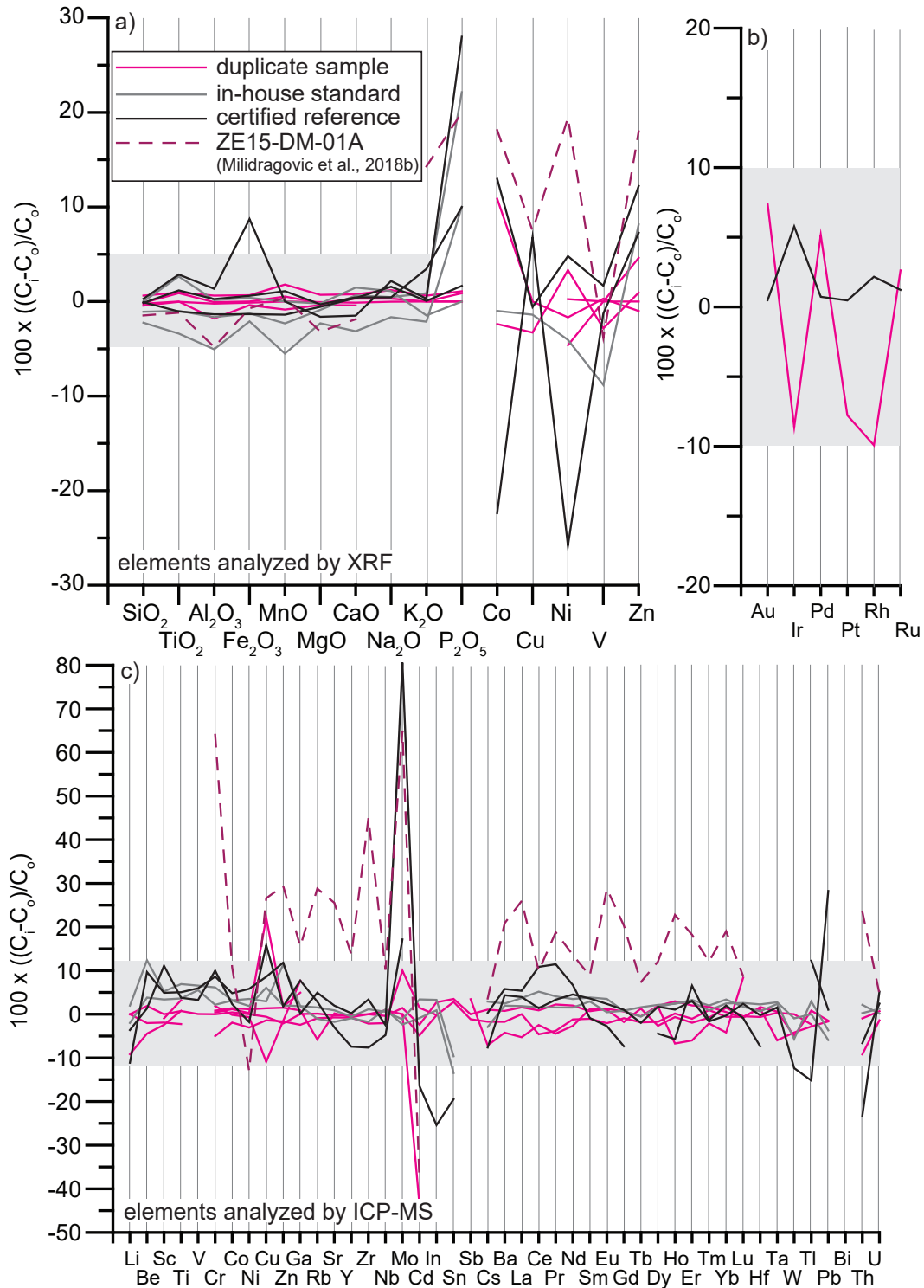


Fig. 3. Diagrams showing the relative uncertainty (in %) in elemental concentrations of samples analyzed in this study. Relative uncertainty is defined as the difference between the measured and reference value for an element, normalized to the reference value. **a)** Major element oxides and selected trace element concentrations determined by XRF. **b)** Gold and platinum group element (PGE) concentrations determined by Ni-S fire assay. **c)** Trace element concentrations determined by ICP-MS.

study area (Fig. 2) are extensively CO_2 -altered ($\text{CO}_2 > 30$ wt.%). Different extents of carbonation have resulted in significant mineralogical variability among listwanite samples (Hansen et al., 2005).

5.2. Geochemistry of the Trembleur ultramafite

The major element chemistry (Table 1) of the relatively unaltered (5.4–10.3 wt.% LOI) Trembleur ultramafite samples ($\text{SiO}_2 = 40.8\text{--}44.4$ wt.%, $\text{MgO} = 43.4\text{--}50.7$ wt.%, $\text{Ni} = 2200\text{--}$

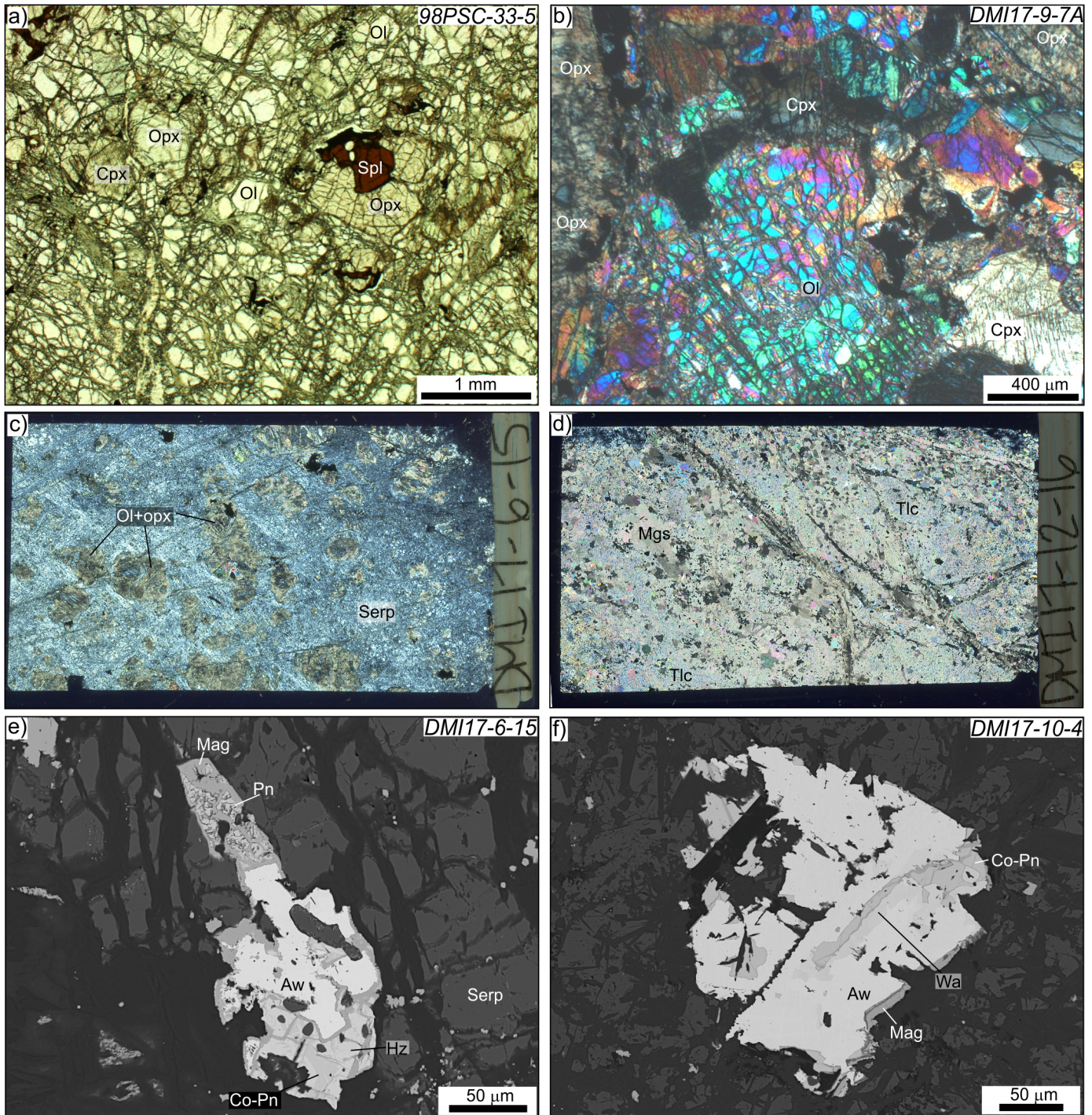


Fig. 4. Representative petrographic images of variably altered Trembleur ultramafite samples from the Decar area. **a)** Plane-polarized light photomicrograph of spinel harzburgite 98PSC-33-5. **b)** Cross-polarized light photomicrograph of spinel harzburgite DMI17-9-7A. **c)** Cross-polarized light scan of serpentine DMI17-6-15 thin section. Light brown ‘enclaves’ in grey massive serpentine are composed of bastite-altered orthopyroxene that has been partly replaced by metamorphic olivine. **d)** Cross-polarized light scan of magnesite-talc listwanite DMI17-12-16 thin section. **e)** Backscattered electron (BSE) image of a composite grain of magnetite (Mag) – pentlandite (Pn) – cobalt-pentlandite (Co-Pn) – heazlewoodite (Hz) – awaruite (Aw) from serpentine DMI17-6-15. **f)** BSE image of composite magnetite (Mag) – cobalt-pentlandite (Co-Pn) – wairuite (Wa) – awaruite (Aw) from serpentine DMI17-10-4.

2900 ppm LOI-free) is consistent with a mineralogy of mainly olivine and orthopyroxene (Figs. 4a-b). Measured LOI contents are consistent with a high degree of serpentinization (40-80%), assuming an H₂O content of anhydrous depleted mantle of

0.116 wt.% (Salters and Strackle, 2004) and H₂O ~13% wt.% in pure serpentine (e.g., Carlson and Miller, 2003). Samples of harzburgite have a limited range of SiO₂ (43.4-45.0 wt.%), MgO (41.8-46.3 wt.%) and FeO^{TOT} (7.8-8.3 wt.%), which

distinguish them from dunite ($\text{SiO}_2 < 41 \text{ wt.}\%$, $\text{MgO} > 50 \text{ wt.}\%$, $\text{FeO}^{\text{TOT}} < 7.5 \text{ wt.}\%$; Figs. 5a-c). Contents of Al_2O_3 (0.6–1.5 wt.%; Fig. 4d) and CaO (0.6–2.8 wt.%) in harzburgite are higher than in dunite, but they are lower than those of the Earth's upper mantle source of mid-ocean ridge basalts (e.g., DM of Salters and Stracke, 2004 or DMM of Workman and Hart, 2005). Measured LOI contents are higher in pervasively serpentinized rocks ($> 10 \text{ wt.}\%$) and carbonate-altered rocks (listwanite; $> 34 \text{ wt.}\%$) compared to relatively unaltered peridotites. In contrast to listwanite ($\text{CO}_2 > 34\text{--}36 \text{ wt.}\%$), serpentinite contains relatively minor CO_2 (0.1–2.6 wt.%). Major element abundances of listwanite and serpentinite, normalized to LOI-free compositions, show significant scatter (Figs. 5a-c), but do not differ systematically from less altered peridotite.

Except for the most mobile trace elements (large ion lithophile elements or LILE, Pb, Sr), the ultramafic rocks of the Decar area have low incompatible trace element abundances ($< 0.3 \times \text{PM}$; primitive mantle of Palme and O'Neill, 2003; Fig. 6a). Middle and heavy rare earth element (MREE and HREE, respectively) abundances, normalized to primitive mantle, show increasing depletion with decreasing atomic number. Limited light REE (LREE) results suggest enrichment of LREE relative to MREE in the Trembleur ultramafite as evidenced by the broadly U-shaped trace element profiles of the analyzed samples (Fig. 6a). There are no systematic differences in trace element contents between the relatively unaltered and serpentinized ultramafic samples (Fig. 6b). This is in contrast to listwanite samples, which display a general depletion in absolute trace element concentrations relative to their harzburgitic protolith, a likely consequence of dilution through carbonate metasomatism.

The abundances of Au and PGE in selected harzburgites and serpentinites of the Trembleur ultramafite (Fig. 6c) are low ($\sim 0.005\text{--}0.02 \times \text{CI-chondrite}$; Palme and O'Neill, 2003), but within the estimated range of abundances in the Earth's depleted upper mantle (Salters and Stracke, 2004). Overall, the iridium-group PGE that were analyzed (Ir, Ru) are not fractionated from the palladium-group PGE (Rh, Pt, Pd).

5.3. Volcanic and shallow intrusive rocks

The volcanic and shallow intrusive rocks of the Decar area have undergone variable deformation and greenschist- to amphibolite-facies metamorphism and recrystallization (Figs. 7, 8). Although primary volcanic structures, such as carbonate or epidote-filled amygdules, are locally recognizable in the field, obscured primary mineralogy and igneous textures are an impediment to petrographic classification and lithostratigraphic unit assignment.

We classify volcanic rocks of the Decar area according to their immobile element concentrations (Fig. 9), following an approach commonly used in petrological investigations of Archean rocks (e.g., Jensen, 1976; Maurice et al., 2003). We define four main geochemical suites (Table 2): 1) high-Ti alkaline; 2) HFSE-depleted; 3) depleted to enriched tholeiitic; and 4) calc-alkaline. Specifying the suite of some samples is ambiguous

because magmatic signatures are modified by alteration and crystal accumulation. For example, samples DMI17-4-10 and DMI17-1-7 are classified as enriched tholeiites based on their extended trace element profiles (Table 2, Fig. 10), although their elevated Th/Yb and Nb/Yb ratios (Fig. 11), suggest a calc-alkaline affinity. Similarly, we classified the coarse-grained sample DMI17-1-5, which is inferred to be a metamorphosed (olivine) clinopyroxenite on the basis of relict clinopyroxene and CaO and MgO-rich composition, as a depleted tholeiite (Fig. 11). However, because of the strong incompatibility of HFSE in clinopyroxene relative to HREE (e.g., Francis and Minarik, 2008), clinopyroxene accumulation lowers the Nb/Yb ratios of resulting cumulate rocks relative to their parental magmas, resulting in a more depleted apparent character. Some of these suites indicate mutually incompatible tectonic settings (e.g., high-Ti alkaline suite and HFSE-depleted suite) and the existence of significant crustal structures. The distribution of volcanic rocks, thus, helps define the position of faults that may mark tectonic boundaries. Furthermore, the suites we define may permit limited regional correlation within the Cache Creek terrane as more geochemical data become available.

5.3.1. High-Ti alkaline suite

High-Ti alkaline samples collected from areas we mapped as Sowchea succession, both east and west of the Trembleur ultramafite (Fig. 2), have variable, but high overall, TiO_2 concentrations (1.5 to 4.1 wt.%; Table 2), which distinguish them from other volcanic suites in the Decar area. The samples have moderate to high LOI (3.3–16.8 wt.%), highly variable SiO_2 (36.9–58.7 wt.%, reported on anhydrous, LOI-free basis), and less variable MgO (3.3–7.0 wt.%), and Al_2O_3 (15.4–19.1 wt.%). The measured range of SiO_2 in the high-Ti alkaline samples spans the compositional spectrum between foidite and trachyandesite. However, classification using immobile elements Zr, Ti, Nb, and Y (Fig. 9a; Pearce, 1996), suggests that all four high-Ti alkaline samples are strongly altered and derived from an alkaline basalt protolith. The defining features of the high-Ti alkaline basalts of the Decar area are the highly fractionated REE profiles ($\text{Ce/Yb}_{\text{MORB}} = 4\text{--}13$, where subscript MORB denotes normalization relative to MORB concentrations of Sun and McDonough, 1989), absolute HREE abundances that are below those of MORB, and enrichment of Nb-Ta relative to the similarly compatible LREE ($\text{Nb/La}_{\text{MORB}} = 1.3\text{--}2.7$; Fig. 10a). The trace element patterns of the high-Ti alkaline basalts overlap those of the Type 2 alkalic basalts of Lapierre et al. (2003), and the Type 3 mafic volcanic rocks from the western belt of the Sitlika assemblage (Schiarizza and Massey, 2010). On the Th/Yb vs. Nb/Yb diagram of Pearce (2008; Fig. 11), alkaline basalts of the Decar area plot within the mantle array, near the average ocean island basalt (OIB) composition (Sun and McDonough, 1989).

5.3.2. HFSE-depleted tholeiitic suite

HFSE-depleted suite samples represent rocks mapped as part of the Rubyrack igneous complex by Struik et al. (2007) and

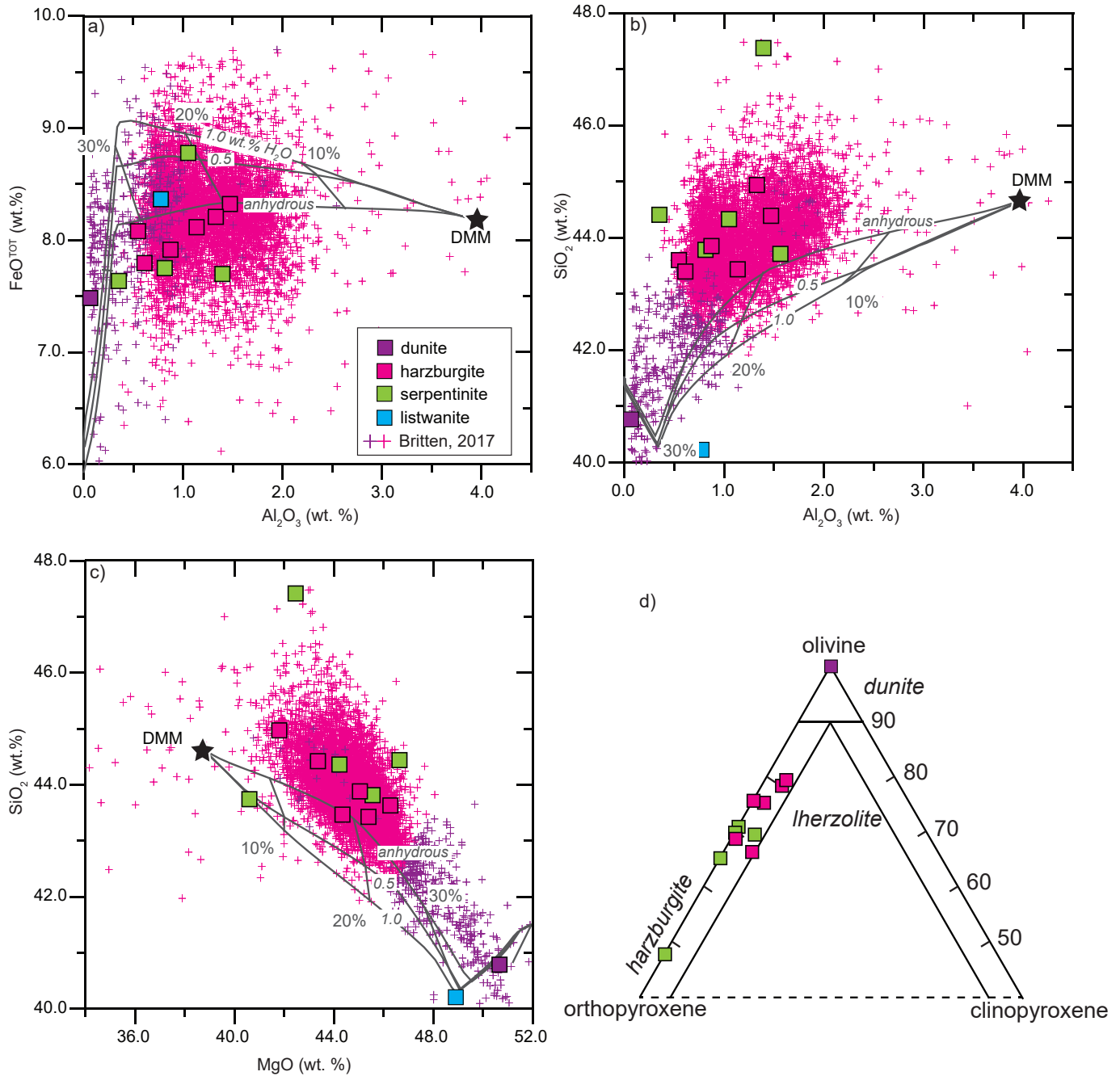


Fig. 5. Whole rock chemistry of Trembleur peridotites. **a)** FeO^{TOT} vs. Al_2O_3 , **b)** SiO_2 vs. Al_2O_3 , **c)** SiO_2 vs. MgO . Also shown are the calculated compositions of residual peridotite formed by 10-30% batch melting of relatively oxidized ($\Delta\log f\text{O}_2 = \text{FMQ}+1$) depleted MORB mantle (DMM; Workman and Hart, 2005) with variable initial water contents (anhydrous, 0.5, and 1.0 wt.%). **d)** Normative (wt.%) olivine-orthopyroxene-clinopyroxene plot of the relatively unaltered and serpentized ultramafic rocks from the Decar area.

Milidragovic et al. (2018a), a gabbro that cuts the Trembleur ultramafite, and rocks previously mapped by Struik et al. (2007) as Sowchea succession on both east and west sides of the Trembleur ultramafite (Fig. 2). These rocks have moderate LOI contents (1.9-5.2 wt.%; Table 2) and variable SiO_2 (43.9-53.9 wt.%), MgO (5.2-11.4 wt.%), and Al_2O_3 (14.0-19.4 wt.%), suggesting a combination of alteration-related mobility and accumulation-differentiation processes. The measured range of

SiO_2 in the HFSE-depleted samples spans the compositional spectrum from micro-basalt to basaltic andesite on the total alkali-silica classification diagram (TAS diagram; LeMaitre, 2005). However, on the Zr/TiO_2 vs. Nb/Y classification diagram (Fig. 9a; Pearce, 1996) the rocks of the HFSE-depleted suite have uniformly basaltic, subalkaline compositions, indicating significant mobility of major elements during metamorphism. On Jensen's (1976) immobile major element classification plot

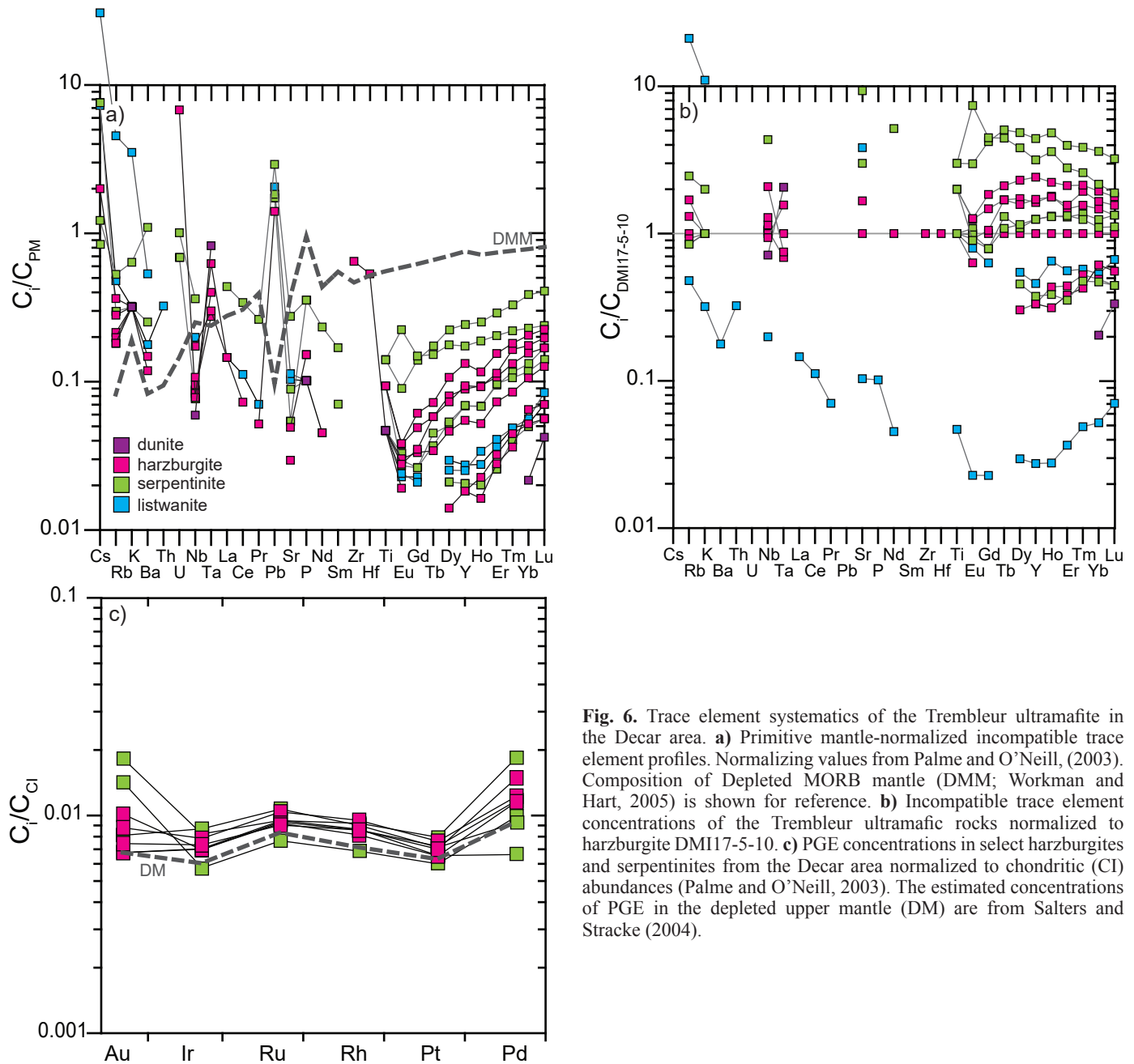


Fig. 6. Trace element systematics of the Trembleur ultramafite in the Decar area. **a)** Primitive mantle-normalized incompatible trace element profiles. Normalizing values from Palme and O'Neill, (2003). Composition of Depleted MORB mantle (DMM; Workman and Hart, 2005) is shown for reference. **b)** Incompatible trace element concentrations of the Trembleur ultramafic rocks normalized to harzburgite DMI17-5-10. **c)** PGE concentrations in select harzburgites and serpentinites from the Decar area normalized to chondritic (CI) abundances (Palme and O'Neill, 2003). The estimated concentrations of PGE in the depleted upper mantle (DM) are from Salters and Stracke (2004).

for subalkaline volcanic rocks (Fig. 9b), all but one HFSE-depleted sample have a tholeiitic affinity.

The HFSE-depleted suite is defined by unfractionated to mildly LREE-depleted MORB-normalized (Sun and McDonough, 1989) trace element patterns coupled with pronounced relative depletions in HFSE (Nb, Ta±Zr, and Hf), and relative enrichments in Th and U (Fig. 10b). Except for one sample, the HFSE-depleted suite has absolute HREE element abundances that are 0.8-1.5 times those of MORB. Although HFSE-depleted tholeiitic basalts were not explicitly identified by Tardy et al. (2001) and Lapierre et al. (2003), our examination of their results reveals that at least four samples (01PG-64, 99CC1, 99CC2; PG96-14), previously classified as

N-MORB and collected north of the town of Cache Creek and from the Pinchi fault near Fort St. James, have HFSE-depleted tholeiitic trace element profiles. On the Th/Yb vs. Nb/Yb diagram (Fig. 11; Pearce, 2008) HFSE-depleted volcanic rocks plot within or slightly above the mantle array and indicate a mantle source that was depleted relative to that of N-MORB.

5.3.3. Depleted to enriched tholeiitic suite

This suite includes a spectrum of altered (LOI=1.9-6.3 wt.%) mafic ($SiO_2=46.7-59.4$; $MgO=5.4-21.3$ wt.%; $Al_2O_3=9.6-19.4$ wt.%) rocks with generally low TiO_2 contents (0.4-2.0 wt.%) and weakly to moderately fractionated trace element patterns. Importantly, these rocks lack the marked depletions





Fig. 7. Field photographs of volcanic and intrusive rocks from the Decar area. **a)** Rusty weathering, veined high-Ti alkaline basalt from the undivided Sowchea succession (Struik et al., 2007) in the southeastern corner of the study area. Sample locality: DMI17-8-4. Rusty colour is due to weathering of cubic pyrite crystals. **b)** Steeply dipping schistosity (upper right to lower left) in an aphanitic, HFSE-depleted tholeiitic basalt, formerly assigned to the greenstone unit of the Sowchea succession in the southwest part of the study area (Struik et al., 2007). Sample locality: DMI17-3-3. **c)** Highly altered (chlorite, carbonate, sericite), and heterogeneously brecciated HFSE-depleted tholeiitic basalt at a small exposure of volcanic rock in the southern portion of Trembleur ultramafite formerly assigned to the Sowchea succession by Struik et al. (2007). Sample locality: DMI17-4-16. **d)** Aphanitic enriched tholeiitic basalt assigned to the greenstone unit of the Sowchea succession in the southwest part of the study area. Sample locality: DMI17-2-9. **e)** Strongly altered and pyrite-rich, aphanitic, enriched tholeiitic basalt with lenses of chert; greenstone unit of the Sowchea succession in the southwest part of the study area (Struik et al., 2007). Sample locality: DMI17-18-5. **f)** Massive, homogeneous plagioclase and clinopyroxene-phyric depleted tholeiitic gabbro from the undivided Sowchea succession (Struik et al., 2007) in the southeastern corner of the study area. Sample locality: DMI17-15-7. **g)** Massive, homogeneous calc-alkaline feldspathic hornblende from a panel of Rubyrock igneous complex in the eastern part of the study area. Sample locality: DMI17-7-6. **h)** Rusty weathering coarse-grained massive calc-alkaline plagioclase-phyric gabbro intruding chert of the Sowchea succession in the southeastern corner of the study area. Sample: DMI17-8-11.

in HFSE that characterize the HFSE-depleted tholeiitic suite. Our samples came mainly from volcanic units we mapped as undivided sedimentary rocks and greenstones of the Sowchea succession, although one sample (DMI17-5-1A) was collected from an outcrop previously assigned (MacIntyre and Schiarizza, 1999; Struik et al., 2007) to the Rubyrock igneous complex and one sample (DMI17-4-10) was from an outcrop previously mapped (MacIntyre and Schiarizza, 1999; Struik et al., 2007) as Trembleur ultramafite (Table 2, Fig. 2). The large compositional range of samples included in this suite is attributed in part to the effects of crystal accumulation (e.g., DMI17-1-5; Fig. 9b), but is also interpreted to reflect differences in magma chemistry arising from mantle source composition and/or melting dynamics. As in the case of high-Ti alkaline and HFSE-depleted tholeiitic suites, classification based on the TAS diagram indicates a wide compositional range of tholeiitic rocks that spans the fields of basalt to andesite. However, immobile trace element concentrations, suggest that at least some of this variability is due to alteration and metamorphism, and that the tholeiitic samples derive from a subalkaline basalt protolith with tholeiitic affinity (Fig. 9). In contrast to the alkaline basalts, tholeiitic basalts show relatively flat MORB-normalized HREE profiles ($Gd/Yb_{MORB}=0.7-1.4$; Fig. 10c), and display both enrichment and depletion in LREE relative to HREE ($Ce/Yb=0.5-3.3$). The trace element patterns of the relatively enriched tholeiitic samples show overlap

with the Type 3 basalts of Lapierre et al. (2003), albeit at a greater range of absolute concentrations (Fig. 10c). Moreover, the depleted to enriched tholeiitic basalts from the Decar area are broadly similar to the mildly depleted to mildly enriched Type 1 tholeiitic basalts and andesites from the eastern belt of the Sitlika assemblage (Schiarizza and MacIntyre, 2010). The tholeiitic samples plot within the mantle array (Fig. 11) and they have Nb/Yb ratios that are intermediate between those of N-MORB and E-MORB (Sun and McDonough, 1989).

5.3.4. Calc-alkaline suite

The three coarse-grained intrusive samples of the calc-alkaline suite have moderate LOI (3.4-6.6 wt.%), variable SiO_2 (46.6-66.0 wt.%) and MgO (1.1-19.0 wt.%), and less variable Al_2O_3 (12.4-16.3 wt.%). The samples have characteristically low TiO_2 contents (0.4-0.9 wt.%). The samples were collected from small outcrops of the Rubyrock igneous complex and the Sowchea succession (Fig. 2). All three outcrops lack the pervasive deformation fabrics typical of the other three volcanic suites, possibly indicating intrusion after the deformation that resulted in the predominant steeply dipping northwest-striking structural trends. When plotted on the Zr/TiO_2 vs. Nb/Y classification diagram (Fig. 9a) the calc-alkaline samples have basaltic to andesitic compositions. Two of the samples have accumulated amphibole±clinopyroxene and consequently plot on the right hand half of the Jansen classification plot (Fig. 9b).

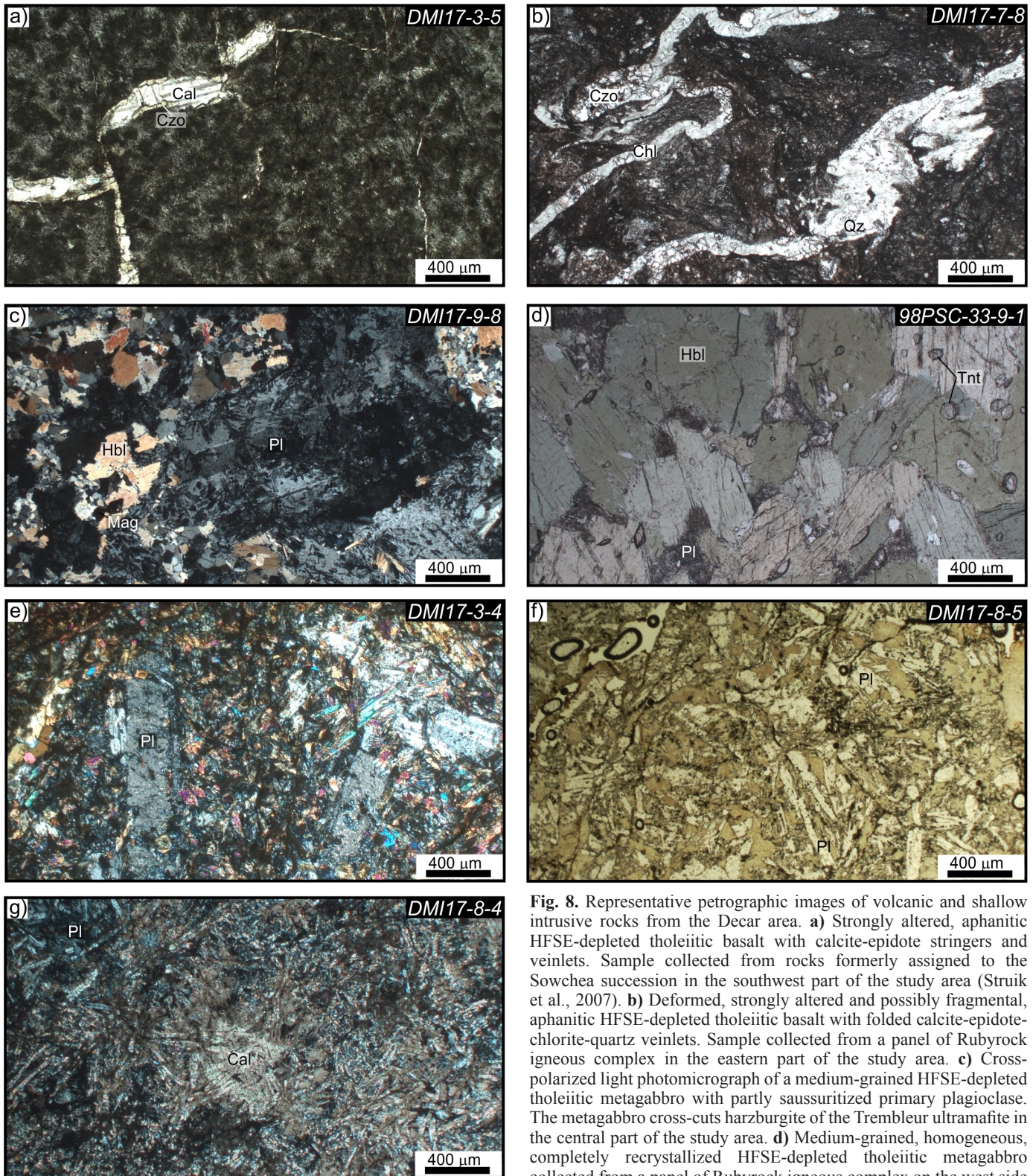


Fig. 8. Representative petrographic images of volcanic and shallow intrusive rocks from the Decar area. **a)** Strongly altered, aphanitic HFSE-depleted tholeiitic basalt with calcite-epidote stringers and veinlets. Sample collected from rocks formerly assigned to the Sowchea succession in the southwest part of the study area (Struik et al., 2007). **b)** Deformed, strongly altered and possibly fragmental, aphanitic HFSE-depleted tholeiitic basalt with folded calcite-epidote-chlorite-quartz veinlets. Sample collected from a panel of Rubyrock igneous complex in the eastern part of the study area. **c)** Cross-polarized light photomicrograph of a medium-grained HFSE-depleted tholeiitic metagabbro with partly saussuritized primary plagioclase. The metagabbro cross-cuts harzburgite of the Trembleur ultramafite in the central part of the study area. **d)** Medium-grained, homogeneous, completely recrystallized HFSE-depleted tholeiitic metagabbro collected from a panel of Rubyrock igneous complex on the west side

of the Trembleur ultramafite. **e)** Fine-grained, plagioclase-phyric high-Ti alkaline basalt from the greenstone unit of the Sowchea succession in the southwest part of the study area. **f)** Medium to coarse-grained, plagioclase-phyric high-Ti alkaline volcanic breccia from the undivided Sowchea succession in the southeastern corner of the study area. **g)** Highly altered (carbonate), plagioclase-phyric high-Ti alkaline basalt from the undivided Sowchea succession in the southeastern corner of the study area. Unless otherwise specified, all photomicrographs are in plane-polarized light.

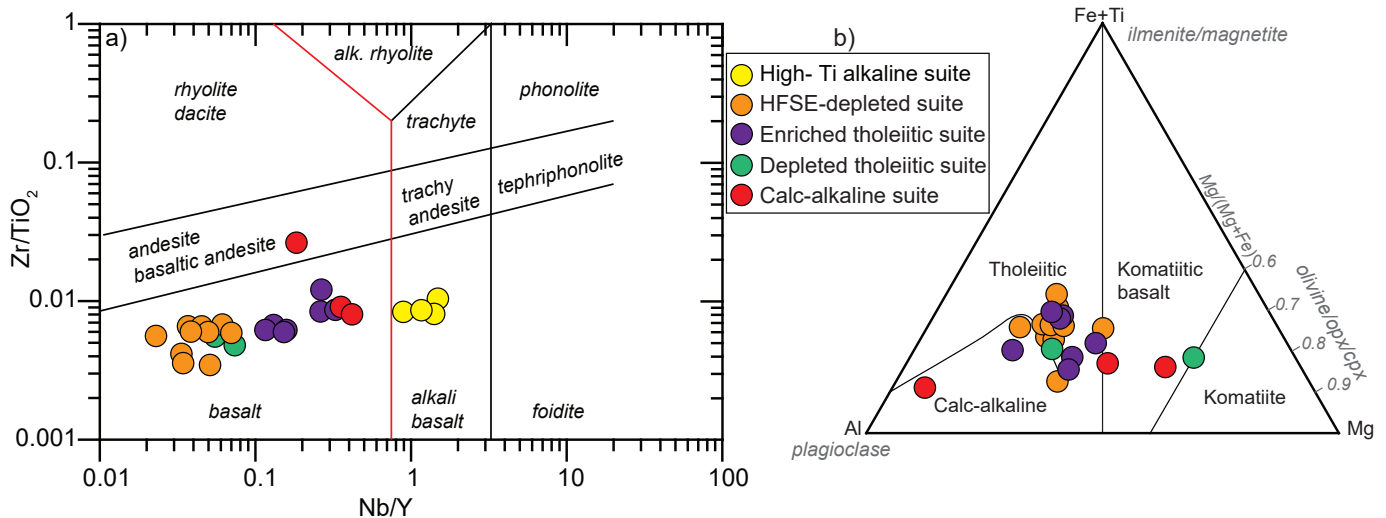


Fig. 9. Classification plots for volcanic and shallow intrusive rocks. **a)** Zr/TiO₂ vs. Nb/Y classification plot for volcanic rocks after Pearce (1996). The red line divides subalkaline from alkaline rocks. **b)** Ternary cation classification plot for subalkaline volcanic rocks after Jensen (1976). Rocks plotting on the right hand side of the triangle are inferred to have accumulated ferromagnesian minerals and are not considered komatiitic.

However, the strongly fractionated trace element patterns and moderate to strong HFSE depletions of all three samples suggest a calc-alkaline magmatic affinity (Fig. 10d).

6. Discussion

6.1. Petrogenesis of the Trembleur ultramafite

The large depletion of Al₂O₃ and CaO relative to depleted upper mantle suggests that the harzburgites of the Decar area are residual mantle rocks formed through significant extraction of basaltic melt. Isobaric batch melting models, performed using alphaMELTS (version 1.8; Ghiorso et al., 2002; Smith and Asimow, 2005) on a relatively oxidized (DlogfO₂=FMQ+1) depleted mantle source (DMM; Workman and Hart, 2005) at 1 GPa suggest that the harzburgites represent residues after ~15-30% melt extraction (Figs. 5a-c). This estimate is higher than the estimation of Grundy (2018) who, using REE concentrations in clinopyroxene and Cr-numbers of spinel (after Hellebrand et al., 2001), suggested that the extent of melting recorded by harzburgites of the Trembleur ultramafite in the Decar area is ~10-15%. This discrepancy in the estimated degree of melting cannot be attributed to the effects of serpentinization because Al₂O₃ is typically immobile during serpentine alteration of peridotite, and harzburgite compositions plotted in Fig. 5 have been corrected for LOI to anhydrous compositions. Furthermore, melt depletion degree estimates that are based on spinel (Hellebrand et al., 2001) and clinopyroxene (Warren, 2016) compositions are highly sensitive to the imposed melting mechanism (batch vs. fractional). Thus at a spinel Cr-number of 0.22 (cf., Grundy, 2018), fractional melting yields a significantly lower melting estimate (~10%) than the batch melting model (~15%). At a spinel Cr-number of 0.3, the discrepancy in melt depletion extent between fractional (~12%) and batch melting (~27%) models is even larger. Although there is no consensus on the melting mechanism

affecting the Trembleur ultramafite, the relatively high degree of depletion implied by low modal and normative abundance of clinopyroxene (Fig. 4d) coupled with the strong depletion of the relatively immobile and incompatible HREE (Fig. 5a) argues against a predominantly fractional melting model.

The relatively low FeO^{TOT} contents of harzburgite samples (<8.3 wt.%) may be explained by melting of dry depleted mantle (Fig. 5a). These samples, as well as the much larger dataset of peridotites from the Decar area reported by Britten (2017; n=5670), have elevated SiO₂ concentrations that significantly exceed the modeled residual compositions (Figs. 5b-c), regardless of the assumed H₂O content or oxygen fugacity. A systematic enrichment in SiO₂ was also observed in spinel-bearing harzburgite and dunite xenoliths from Kamchatka and Bismarck arcs by Bénard et al. (2017). The SiO₂-enrichment of the peridotite xenoliths from the western Pacific, as well as the high modal orthopyroxene abundance in mantle xenoliths from volcanic arcs (Parkinson and Pearce, 1998; Ionov, 2010) in general, were interpreted by Bénard et al. (2017) to be a defining feature of sub-arc mantle attributable to metasomatism of refractory mantle by slab-derived fluids and/or melts. Accordingly, the relatively high SiO₂ concentration and high modal proportion of orthopyroxene (17-30%) in harzburgites of the Decar area are interpreted to reflect a silica-enriched refractory mantle source. Given the apparent prevalence of such mantle under modern-day arcs, we propose that the Trembleur ultramafite developed in a supra-subduction zone setting.

6.2. Lithostratigraphic reassignment of outcrops in the Decar area using the geochemistry of volcanic suites

The geochemical data presented herein can be used to assign outcrops to lithostratigraphic units that are otherwise difficult to distinguish in the field. Two samples in the southwestern part

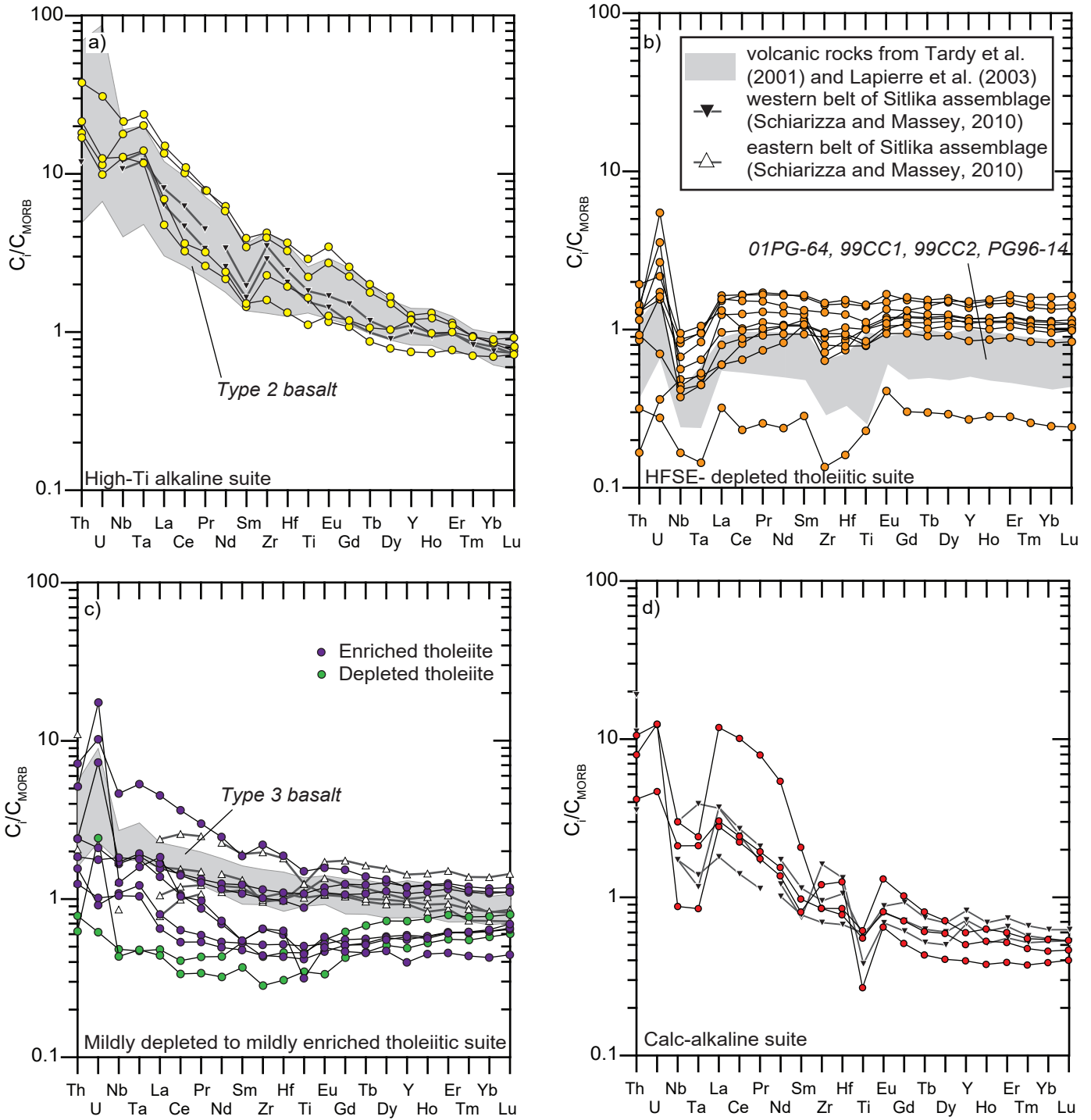


Fig. 10. MORB-normalized trace element patterns of the volcanic and shallow intrusive rocks from the Decar area. Normalization values from Sun and McDonough (1989). **a)** High-Ti alkaline suite compared to the Type 2 alkaline basalts from the Cache Creek terrane in central British Columbia (Lapierre et al., 2003) and Type 3 mafic volcanic rocks from the western belt of the Sitlika assemblage (Schiarizza and Massey, 2010). **b)** HFSE-depleted tholeiitic suite. Also shown is the compositional range of HFSE-depleted samples assigned to Type 1 N-MORB suite by Lapierre et al. (2003). **c)** Mildly depleted and mildly enriched tholeiitic suite. Shown for comparison are the Type 3 oceanic plateau basalts of Lapierre et al., 2003 and the Type 1 volcanics from the eastern belt of the Sitlika assemblage (Schiarizza and Massey, 2010). **d)** Calc-alkaline suite. Type 2 volcanic rocks from the western belt of the Sitlika assemblage (Schiarizza and Massey, 2010) are shown for comparison.

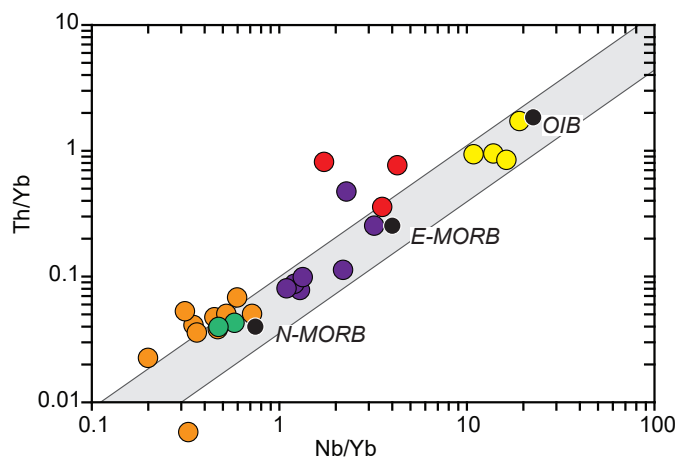


Fig. 11. Plot of Th/Yb vs. Nb/Yb after Pearce (2008), showing the wide compositional range of volcanic and shallow intrusive rocks of the Decar area and superimposed on the MORB-OIB array (grey field). The average compositions of N-MORB, E-MORB, and OIB are from Sun and McDonough (1989). Symbols as in Fig. 9.

of the Decar area (DMI17-3-3 and DMI17-3-5), which display HFSE-depleted tholeiitic suite geochemistry (Fig. 2; Table 2), redefine the geometry of the panel of rocks previously mapped as the Rubyrock igneous complex by Struik et al. (2007). A sample of schistose aphanitic metabasalt on the western edge of the study area (sample DMI17-2-15) is distinguished from the aforementioned samples by its enriched tholeiitic geochemical signature and indicates a previously unmapped (MacIntyre and Schiarizza, 1999; Struik et al., 2007) panel of volcanic rocks that lack a subduction signature in the westernmost part of the Decar area. Consequently, this panel is assigned to the Sowchea succession, necessitating a fault that separates the two geochemically distinct volcanic units.

6.3. Tectonic significance

Previous interpretations from the southern segment of the Cache Creek terrane (Tardy et al., 2001; Lapierre et al., 2003) emphasized the prevalence of volcanic rocks with alkaline to mildly depleted tholeiitic trace element patterns and argued that most volcanic rocks of the Cache Creek complex erupted in an oceanic plateau setting and were mantle plume derived. Our Sowchea succession data, which indicate an alkaline to mildly LREE-enriched to mildly LREE-depleted tholeiitic geochemistry (Figs. 2, 9-11), largely support this interpretation. However, our data also contradict this interpretation by identifying an HFSE-depleted volcanic component typical of island arc tholeiite (IAT) magmas in the Rubyrock igneous complex (Figs. 9-10). We conclude that the Cache Creek terrane in central British Columbia is not merely a tectonic amalgamation of mantle plume-related oceanic plateau rocks and suggest that, based on our results, the contrasting geochemical signatures in the southern segment of the Cache Creek terrane (e.g., Type 2 and 3 volcanic rocks, western belt of Sitlika assemblage of Schiarizza and MacIntyre, 2010) warrant re-evaluation. Our results support the conclusion of McGoldrick et al. (2017) who

interpreted that supracrustal volcanic and plutonic rocks in the northern segment of the Cache Creek terrane mainly represent the product of an intraoceanic arc, with only a minor intraplate oceanic component.

The IAT crustal affinity of the Rubyrock igneous complex and the anomalous SiO_2 enrichment of the adjacent mantle harzburgite (Trembleur ultramafite) are consistent with the view that the two units represent crustal and mantle segments of a dismembered supra-subduction ophiolitic complex (Schiarizza and MacIntyre, 1999; Struik et al., 2001; Britten, 2017). This supra-subduction zone setting is incompatible with the intraoceanic (OIB-E-MORB-N-MORB, Fig. 11) basalt geochemistry of volcanic rocks in the Sowchea succession. The oceanic plateau affinity of the volcanic rocks and associated carbonate rocks, cherts, and argillites of the Sowchea succession suggests that these rocks formed in an unrelated tectonic setting and that they were likely sliced off the subducting 'Cache Creek ocean' during its Jurassic closure (Nelson et al., 2013). Therefore, we propose that the term 'Cache Creek complex' be restricted to include only those lower plate rocks that lack a supra-subduction zone signature (cf., Struik et al., 2001). Future work will evaluate links between units formed on the upper plate of the convergent margin such as the Trembleur ultramafite and Rubyrock igneous complex in the Decar area, and the Kutcho-Sitlika-Venables arc (Permo-Triassic, e.g., Logan and Mihalynuk, 2014) farther north in the Cache Creek terrane.

7. Summary

The geochemistry of variably serpentinized and carbonate-altered mantle tectonite and greenschist- to amphibolite-facies mafic to intermediate igneous rocks from the Decar area in central British Columbia provide new evidence of two distinct tectono-stratigraphic assemblages in the Cache Creek complex. Volcanic and intrusive rocks with alkaline to mildly LREE-depleted tholeiitic chemistry and associated limestone, chert, and argillite comprising the Sowchea succession (Upper Pennsylvanian to Lower Jurassic) may have been deposited in an oceanic plateau setting (Tardy et al., 2001; Struik et al., 2001; Lapierre et al., 2003) and resided on the lower plate during the Jurassic closure of the Cache Creek ocean. In contrast, the high- SiO_2 refractory mantle peridotite of the Trembleur ultramafite and the overlying supracrustal rocks with a predominant island arc tholeiite component originated in an upper plate, suprasubduction zone setting. These tectono-stratigraphic packages were likely juxtaposed and interleaved during the collision between the Cache Creek terrane and Stikinia in the Late Jurassic (Struik et al., 2001; English and Johnston, 2005).

Acknowledgments

We thank Tl'azt'en Nation and Chief Bev John for hospitality and FPX Nickel Corp. and Ron Britten for sharing their geochemical and geophysical data with us. Alan King (Geoscience North) is thanked for processing the aeromagnetic

survey data provided by FPX Nickel Corp. We thank A. Zagorevski and J. Scoates for their helpful and constructive reviews.

References cited

- Armstrong, J.E., 1949. Fort St. James map-area, Cassiar and Coast Districts, British Columbia. Geological Survey of Canada, Memoir 252. 210 p.
- Bénard, A., Arculus, R.J., Nebel, O., Ionov, D.A., and McAlpine, S.R.B., 2017. Silica-enriched mantle sources of subalkaline picrite-boninite-andesite island arc magmas. *Geochimica et Cosmochimica Acta*, 199, 287-303.
- Boudier, F., and Nicolas, A., 1985. Harzburgite and lherzolite subtypes in ophiolitic and oceanic environments. *Earth and Planetary Science Letters*, 76, 84-92.
- Britten, R., 2017. Regional metallogeny and genesis of a new deposit type-disseminated awaruite (Ni₃Fe) mineralization hosted in the Cache Creek terrane. *Economic Geology*, 112, 517-550.
- Canil, D., Johnston, S.T., and Mihalynuk, M., 2006. Mantle redox in Cordilleran ophiolites as a record of oxygen fugacity during partial melting and the lifetime of mantle lithosphere. *Earth and Planetary Science Letters*, 248, 91-102.
- Carlson, R.L., and Miller, D.J., 2003. Mantle wedge water contents estimated from seismic velocities in partially serpentinized peridotites. *Geophysical Research Letters*, 30, 1250-1253.
- Childe, F.C., and Schiarizza, P., 1997. U-Pb geochronology, geochemistry and Nd isotopic systematics of the Sitlika assemblage, central British Columbia. In: *Geological Fieldwork 1996*, British Columbia Ministry of Energy, Mines and Petroleum Resources, Paper 1997-1, pp. 69-77.
- Childe, F.C., and Thompson, J.F.H., 1997. Geological setting, U-Pb geochronology, and radiogenic isotopic characteristics of the Permo-Triassic Kutcho assemblage, north-central British Columbia. *Canadian Journal of Earth Sciences*, 34, 1310-1324.
- Cordey, F., Gordey, S.P., and Orchard, M.J., 1991. New biostratigraphic data from the northern Cache Creek terrane, Teslin map area, southern Yukon. In: *Current research part E. Geological Survey of Canada*, pp. 67-76.
- Elliot, A.J.M., 1975. *Geology and metamorphism of the Mitchell Mountains ultramafite, Fort St. James map area, British Columbia*. Unpublished M.Sc. thesis, The University of British Columbia, Vancouver, B.C., 129 p.
- English, J.M., and Johnston, S.T., 2005. Collisional orogenesis in the northern Canadian Cordillera: Implications for Cordilleran crustal structure, ophiolite emplacement, continental growth, and the terrane hypothesis. *Earth and Planetary Science Letters*, 232, 333-344.
- English, J.M., Mihalynuk, M.G., and Johnston, S.T., 2010. Geochemistry of the northern Cache Creek terrane and implications for accretionary processes in the Canadian Cordillera. *Canadian Journal of Earth Sciences*, 47, 13-34.
- Francis, D., and Minarik, W., 2008. Aluminum-dependent trace element partitioning in clinopyroxene. *Contributions to Mineralogy and Petrology*, 156, 439-451.
- Ghiorso, M. S., Hirschmann, M.M., Reiners, P.W., and Kress, V.C., 2002. The pMELTS: A revision of MELTS for improved calculation of phase relations and major element partitioning related to partial melting of the mantle to 3GPa. *Geochemistry, Geophysics, Geosystems*, 3, 1030. doi: 10.1029/2001GC000217.
- Golding, M.L., 2018. Heterogeneity of conodont faunas in the Cache Creek Terrane, Canada; significance for tectonic reconstructions of the North American Cordillera. *Palaeogeography, Palaeoclimatology, Palaeoecology*, 506, 208-216.
- Golding, M.L., Orchard, M.J., and Zagorevski, A., 2016. Microfossils from the Cache Creek Complex in northern British Columbia and southern Yukon. Geological Survey of Canada, Open File 8033, 25 p.
- Grundy, R., 2018. Melting and cooling histories of two upper mantle massifs in the Cache Creek Terrane, central British Columbia. Unpublished B.Sc. Thesis, University of Victoria, 60 p.
- Hansen, L.D., Dipple, G.M., Gordon, T.M., and Kellett, D.A., 2005. Carbonated serpentinite (listwanite) at Atlin, British Columbia: a geological analogue to carbon dioxide sequestration. *Canadian Mineralogist*, 43, 225-239.
- Harte, B., 1977. Rock nomenclature with particular relation to deformation and recrystallisation textures in olivine-bearing xenoliths. *Geology*, 85, 279-288.
- Hellebrand, E., Snow, J.E., Dick, H.J.B., and Hofmann, A.W., 2001. Coupled major and trace elements as indicators of melting in mid-ocean ridge peridotites. *Nature*, 410, 677-681.
- Ionov, D.A., 2010. Petrology of mantle wedge lithosphere: new data on supra-subduction zone peridotite xenoliths from the andesitic Avacha volcano, Kamchatka. *Journal of Petrology*, 51, 327-361.
- Jensen, L.S., 1976. A new cation plot for classifying subalkalic volcanic rocks. Ontario Ministry of Natural Resources, Division of Mines, Miscellaneous Paper 66, 22 p.
- Lapierre, H., Bosch, D., Tardy, M., and Struik, L.C., 2003. Late Paleozoic and Triassic plume-derived magmas in the Canadian Cordillera played a key role in continental crust growth. *Chemical Geology*, 201, 55-89.
- LeMaitre, R.W., 2005. *Igneous Rocks: A Classification and Glossary of Terms*. In: R.W. LeMaitre (Ed.), *Recommendations of the International Union of Geological Sciences Subcommittee on the Systematics of Igneous Rocks (2nd edition)*. Cambridge University Press, 236 p.
- Logan, J.M., and Mihalynuk, M.G., 2014. Tectonic controls on early Mesozoic paired alkaline porphyry deposit belts (Cu-Au±Ag-Pt-Pd-Mo) within the Canadian Cordillera. *Economic Geology*, 109, 827-858.
- MacIntyre, D.M., and Schiarizza, P., 1999. Bedrock geology, Cunningham Lake (93K/11, 12, 13, 14). British Columbia Ministry of Energy and Mines, British Columbia Geological Survey Open File 1999-11; scale 1:100,000.
- McGoldrick, S., Zagorevski, A., and Canil, D., 2017. Geochemistry of volcanic and plutonic rocks from the Nahlin ophiolite with implications for a Permo-Triassic arc in the Cache Creek terrane, northwestern British Columbia. *Canadian Journal of Earth Sciences*, 54, 1214-1227.
- McGoldrick, S., Canil, D., and Zagorevski, A., 2018. Contrasting thermal histories for segments of mantle lithosphere in the Nahlin ophiolite, British Columbia, Canada. *Contributions to Mineralogy and Petrology*, 173:25, 17 p.
- Maurice, C., Francis, D., and Madore, L., 2003. Constraints on early Archean crustal extraction and tholeiitic-komatiitic volcanism in greenstone belts of the Northern Superior Province. *Canadian Journal of Earth Sciences*, 40, 431-445.
- Mercier, J.C.C., and Nicolas, A., 1975. Textures and fabrics of upper-mantle peridotites as illustrated by xenoliths from basalts. *Journal of Petrology*, 16, 454-487.
- Milidragovic, D., Grundy, R., and Schiarizza, P., 2018a. Geology of the Decar area north of Trembleur Lake, NTS 93K/14. In: *Geological Fieldwork 2017*, British Columbia Ministry of Energy, Mines and Petroleum Resources, British Columbia Geological Survey Paper 2018-1, pp. 129-142.
- Milidragovic, D., Zagorevski, A., Weis, D., Joyce, N., and Chapman, J.B., 2018b. Picrite “intelligence” from the Middle-Late Triassic Stikine arc: Composition of mantle wedge asthenosphere. *Lithos*, 308-309, 446-461.
- Monger, J.W.H., 1975. Upper Paleozoic rocks of the Atlin terrane, northwestern British Columbia and south-central Yukon. Geological Survey of Canada, Paper 74-47, 63 p.

- Monger, J.W.H., 1977. Upper Paleozoic rocks of the western Canadian Cordillera and their bearing on Cordilleran evolution. *Canadian Journal of Earth Sciences*, 14, 1832-1859.
- Monger, J.W.H., and Ross, C.A., 1971. Distribution of fusulinaceans in the western Canadian Cordillera. *Canadian Journal of Earth Sciences*, 8, 259-278.
- Mihalynuk, M.G., Nelson, J.L., and Diakow, L.J., 1994. Cache Creek terrane entrapment: Oroclinal paradox within the Canadian Cordillera. *Tectonics*, 13, 575-595.
- Nelson, J.L., Colpron, M., and Israel, S., 2013. The Cordillera of British Columbia, Yukon, and Alaska: Tectonics and metallogeny. In: Colpron, M., Bissing, T., Rusk, B.G., and Thompson, J.F.H., (Eds.), *Tectonics, Metallogeny, and Discovery: The North American Cordillera and Similar Accretionary Settings*. Society of Economic Geologists, Special Publication 17, pp. 53-109.
- Orchard, M.J., Cordey, F., Rui, L., Bamber, E.W., Mamet, B., Struik, L.C., Sano, H., and Taylor, H.J., 2001. Biostratigraphic and biogeographic constraints on the Carboniferous to Jurassic Cache Creek terrane in central British Columbia. *Canadian Journal of Earth Sciences*, 38, 551-578.
- Palme, H., and O'Neill, H.St.C., 2003. Cosmochemical estimates of mantle composition. In: Holland, H.D., Turekian, K.K., and Davis, A.M. (Eds.), *Treatise on Geochemistry*, Vol. 2. Elsevier, Amsterdam, The Netherlands, pp. 1-38.
- Parkinson I.J., and Pearce J.A., 1998. Peridotites from the Izu-Bonin-Mariana forearc (ODP leg 125): evidence for mantle melting and melt-mantle interaction in a supra-subduction zone setting. *Journal of Petrology*, 39, 1577-1618.
- Paterson, I.A., 1977. The geology and evolution of the Pinchi Fault Zone at Pinchi Lake, central British Columbia. *Canadian Journal of Earth Sciences*, 14, 1324-1342.
- Pearce, J.A., 1996. A user's guide to basalt discrimination diagrams. In: Wyman D.A., (Ed.), *Trace Element Geochemistry of Volcanic Rocks: Applications for Massive Sulphide Exploration*. Geological Association of Canada, Short Course Notes, 12, pp. 79-113.
- Pearce, J.A., 2008. Geochemical fingerprinting of oceanic basalts with applications to ophiolite classification and the search for Archean oceanic crust. *Lithos*, 100, 14-48.
- Salters, V.J., and Stracke, A., 2004. Composition of the depleted mantle. *Geochemistry, Geophysics, geosystems*, 5, Q05B07, doi:10.1029/2003GC000597.
- Schiarizza, P., 2012. Geology of the Kutcho Assemblage between the Kehlechoa and Tucho Rivers, Northern British Columbia (NTS 104I/01, 02). In: *Geological Fieldwork 2011*, British Columbia Ministry of Energy and Mines, British Columbia Geological Survey Paper 2012-1, pp. 75-98.
- Schiarizza, P., and MacIntyre, D.G., 1999. Geology of the Babine Lake-Takla Lake area, central British Columbia (93K/11, 12, 13, 14; 93N/3, 4, 5, 6). In: *Geological Fieldwork 1998*, British Columbia Ministry of Energy and Mines, British Columbia Geological Survey Paper 1999-1, pp. 33-68.
- Schiarizza, P., and Massey, N.W.D., 2010. Geochemistry of volcanic and plutonic rocks of the Sitlika assemblage, Takla Lake area, central British Columbia (NTS 093N/04, 05, 12, 13). In: *Geological Fieldwork 2009*, British Columbia Ministry of Energy, Mines and Petroleum Resources, British Columbia Geological Survey Paper 2010-1, pp. 55-67.
- Smith, P.M., and Asimow, P.D., 2005. Adibat_1ph: A new public front- end to the MELTS, pMELTS, and pHMELTS models. *Geochemistry, Geophysics, Geosystems*, 6, Q02004, doi:10.1029/2004GC000816.
- Struik, L., Schiarizza, P., Orchard, M., Cordey, F., Sano, H., MacIntyre, D.G., Lapierre, H., and Tardy, M., 2001. Imbricate architecture of the upper Paleozoic to Jurassic oceanic Cache Creek terrane, central British Columbia. *Canadian Journal of Earth Sciences*, 38, 495-514.
- Struik, L.C., MacIntyre, D.G., and Williams, S.P., 2007. Nechako NATMAP project: A digital suite of geoscience information for central British Columbia. Geological Survey of Canada Open File 5623.
- Sun, S., and McDonough, W.F., 1989. Chemical and isotopic systematics of oceanic basalts: implications for mantle composition and processes. In: Saunders, A.D., and Norry, M.J. (Eds.), *Magmatism in the Ocean Basins*, Geological Society of London, Special Publication 42, 313-345.
- Tardy, M., Lapierre, H., Struik, L.C., Bosch, D., and Brunet, P., 2001. The influence of mantle plume in the genesis of the Cache Creek oceanic igneous rocks: implications for the geodynamic evolution of the inner accreted terranes of the Canadian Cordillera. *Canadian Journal of Earth Sciences*, 38, 515-534.
- Voordouw, R.J., and Simpson, R.G., 2018. 2018 technical (N.I. 43-101) report on the Decar nickel-iron alloy property. Independent technical report, 81 p. https://fpxnickel.com/wp-content/uploads/2018/04/2018_Decar_NI43101.pdf (Last accessed Dec.4th, 2018).
- Warren, J.M., 2016. Global variation in abyssal peridotite compositions. *Lithos*, 248-251, 193-219.
- Workman, R.K., and Hart, S.R., 2005. Major and trace element composition of the depleted MORB mantle (DMM). *Earth and Planetary Science Letters*, 231, 53-72.